Magnetic field extrapolations

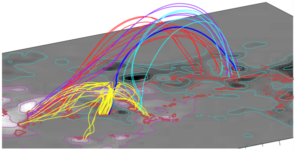

Gherardo Valori

UCL MSSL

4th SOLARNET Summer School on Solar MHD and Reconnection

13-19 April 2016, MSSL

Outline

Coronal field

The coronal magnetic field is responsible for

- connection between Sun and interplanetary space
- channelling Sun's disturbances through space
- up to near-Earth environment, and beyond

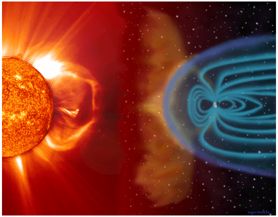

Courtesy of ESA

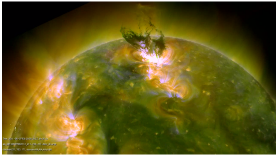

Courtesy of K. Schrijver

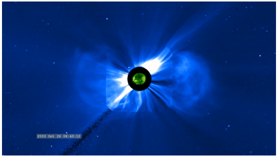

Halloween 2003

CMEs: Rearrangement of the low-atmospheric magnetic field on a minute time-scale with virulent ejection of field and material (filaments), and often accompanied by flares

CMEs/flares are essential to understand the removal of energy and helicity emerging through the Sun surface

UCL MSSL

Extrapolation

- **The 3D structure of the coronal field is necessary**
  - low-corona: to validate CME models
  - solar wind interaction and interplanetary connection (channeling)
- Event forecast must be able to evolve real configurations forwards in time

Few hundreds km above the photosphere, estimations of $\vec{B}$ are available

- at points or line (*e.g.*, Farady rotation of emission from extragalactic radio sources Mancuso *et al.*, A&A 2013)
- on the limb (*e.g.*, from CoMP but partial information only)
- in situ (at 1AU, these are the only direct measurements)

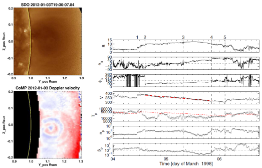

Field in a prominence cavity (Bąk-Stęślicka *et al.*, ApJ 2013), and at 1AU (Nakwacki *et al.*, A&A 2011)

But the 3D information is missing
The magnetic vector field can be measured with sufficient accuracy, resolution, and time cadence only at the photosphere

Extrapolation of photospheric measurements into the solar atmosphere is the main technique for obtaining the full 3D structure of the coronal field

Deduce $\vec{B}$ in whatever volume from its footprint at the bottom boundary $\Longrightarrow$ it requires a model

The quasi-static corona

The average density difference between low-corona and photosphere

$$n_{\mathrm{ph}}/n_{\mathrm{c}} \sim 10^8$$

is not matched by any comparable jump in magnetic field $\Longrightarrow$

- the photosphere evolve on a long time scale of hours to days
- the corona, with much lower density, evolve on fast time scale (Alfvén time order of seconds)

i.e., the coronal field instantaneously adapts to the slow photospheric changes

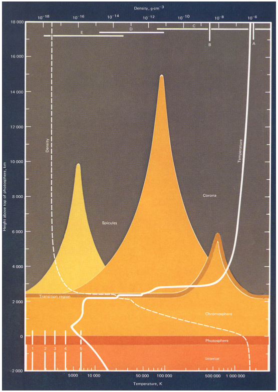

Density (dashes) vs height above the photosphere (SKYLAB, courtesy of NASA)

$\Longrightarrow$ the corona evolves as a series of quasi-static equilibria (except at times of fast events, *e.g.*, eruptions)

The magnetically-dominated corona

Energy requirement of a moderately large CME

Parameter	Value
Kinetic energy (CME, Prominence, & shock)	10^{32} erg
Heating & radiation	10^{32} erg
Work done against gravity	10^{32} erg
Volume involved	10^{30} cm^3
Energy density	100 erg cm^{-3}

Estimates of coronal energy sources

Form of Energy	Obs. average values	Energy density erg cm^{-3}
Kinetic ($m_p n V^2/2$)	$n = 10^9$ cm^{-3}; $V = 1$ km s^{-1}	10^{-5}
Thermal ($2nkT$)	$T = 10^6$ K	0.2
Gravitational ($m_p n g h$)	$h = 10^5$ km	0.5
Magnetic ($B^2/2\mu_0$)	$B = 100$ G	400

Kliem, adapted from Forbes JGR 2000

The energy liberated by a (medium sized) CME can originate only from magnetic sources

Variation of plasma $\beta = \dfrac{\text{plasma pressure}}{\text{magnetic pressure}} = 2\mu_0 \dfrac{p}{B^2}$ with altitude

- low corona (*i.e.*, up to $\sim$1.5 $R_\odot$) has $\beta < 1$
  $\Longrightarrow$ magnetic forces dominate over pressure gradients
- except in particular locations (*e.g.*, thin current sheets, instrumentally undetectable)

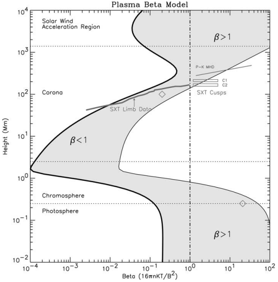

Gary, Sol. Phys. 2001

Magnetic field dominates all other sources of energy
$\Longrightarrow$ no possible balance of the Lorentz force

Coronal currents

Currents in the low corona are local, *e.g.*, are found

- at low altitudes, up to chromospheric layers
- in/around filaments, sheared arcades, erupting and flaring structures
- higher, at particular locations (*e.g.*, helmet streamers, heliospheric current sheet)

On the other hand, Thomson theorem proves that the potential field is the minimal energy state

$\Longrightarrow$ $E - E_{\rm p}$ = free energy (*i.e.*, currents) must be stored in coronal pre-erupting structures!

Thomson theorem

By decomposing the field $\vec{B}$ as the sum of potential, $\vec{B}_{\rm p} = \vec{\nabla}\phi$, and current carrying, $\vec{B}_{\rm J}$ with $\vec{J} = \vec{\nabla} \times \vec{B}_{\rm J}$,

$$\vec{B} = \vec{B}_{\rm p} + \vec{B}_{\rm J} \ ,$$

the total magnetic energy E in a volume $\mathcal{V}$ is given by

$$E \equiv \frac{1}{2}\int_{\mathcal{V}} dV\, B^2 = E_{\rm p} + E_{\rm J} + \int_{\partial\mathcal{V}} (\phi\vec{B}_{\rm J}) \cdot {\rm d}\vec{S} - \int_{\mathcal{V}} \phi(\vec{\nabla}\cdot\vec{B}_{\rm J})\,{\rm d}\mathcal{V} \ ,$$

where $E_{\rm p} \equiv \frac{1}{2}\int_{\mathcal{V}} B_{\rm p}^2\,{\rm d}\mathcal{V}$, $E_{\rm J} \equiv \frac{1}{2}\int_{\mathcal{V}} B_J^2\,{\rm d}\mathcal{V}$, $\partial\mathcal{V}$ is the boundary of $\mathcal{V}$, ${\rm d}\vec{S} = \hat{n}\,{\rm d}S$, and $\hat{n}$ is the external normal to $\partial\mathcal{V}$

1. If $\hat{n}\cdot(\vec{B} - \vec{B}_{\rm p})|_{\partial\mathcal{V}} = 0 \Longrightarrow \hat{n}\cdot\vec{B}_{\rm J}|_{\partial\mathcal{V}} = 0$
2. $\vec{\nabla}\cdot\vec{B}_{\rm J} = 0$ from Maxwell

then $E = E_{\rm p} + E_{\rm J}$,

$\Longrightarrow$ the energy of a magnetic field is bounded from below by the energy of the corresponding potential field that has the same distribution of the normal component on the boundary of the considered volume.

NB: at any time, for any plasma.

The force-free model

To first approximation, the low-corona is

1. static on the $\tau_{\rm ph}$ time scale $\Longrightarrow$ $\partial_t \simeq 0$, $\frac{L_{\rm B}}{L_{\rm v}} M_A^2 \ll 1$
2. magnetically dominated $\Longrightarrow$ $\frac{L_{\rm B}}{L_{\rm p}} \beta \ll 1$
3. with essential but concentrated currents ($\vec{J} = \vec{\nabla} \times \vec{B} \neq 0$)

The (ideal MHD) momentum balance equation

$$\rho \left(\partial_t + \vec{v} \cdot \vec{\nabla} \right) \vec{v} + \vec{\nabla} p = \vec{J} \times \vec{B}$$

reduces to the force free equation, coupled with the solenoidal condition for $\vec{B}$

$$\begin{cases} \vec{J} \times \vec{B} = 0 \,, \\ \vec{\nabla} \cdot \vec{B} = 0 \end{cases}$$

- nasty BVP of coupled nonlinear PDEs (elliptic/hyperbolic), despite its innocent look
- to be solved subjected to photospheric (*i.e.*, not force-free-compatible) BC

It is *not* a vacuum field ($\vec{J} = \vec{\nabla} \times \vec{B}$ requires a plasma), but it is insensitive to inertia and pressure gradients

Magnetograms

The “standard", *i.e.*, photospheric, magnetograms (mgm) come in two types

LoS mgm

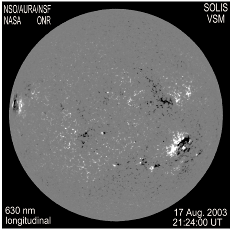

SOLIS LoS mgm

- From magnetographs, imaging techniques
- Full disk and fast (up to 45 seconds cadence)
- Measure the component of the field in the direction of the observer (Line of Sight, LoS)
- Huge historical databases available (essential for statistics)

Vector mgm

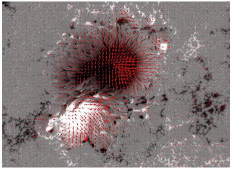

AR10930 Hinode/SOT 12 Dec 2006

- Spectropolarimetric observations come from an iso-τ surface at photospheric heights
- $\vec{B}$ is inferred fitting the full spectral profiles of the Stokes parameters (requires atmospheric models)
- Measure LoS, magnitude and orientation of the transverse component, *i.e.*, almost the full vector (180deg ambiguity)
- 12min to hour cadence
  high spatial resolution (at most 0.16 arcsec) high nominal accuracy (few G/few tens G on $\parallel$ / $\perp$)

The photosphere is not force-free ($\beta \geq 1$), the field above ARs becomes force-free above $\simeq$ 400 km (Metcalf *et al.*, ApJ 1995)

UCL MSSL

FF eqs with nonFF BC?

Extrapolation, as a boundary value problem (BVP), is well-posed if it can be proved

Existence	of the solution Important because part of boundary data come from a finite-β plasma $\Longrightarrow$ a solution may simply not exist
Uniqueness	of the solution Important because different sets of field lines might be possible for the same set of footpoints $\Longrightarrow$ multiple solutions may be possible
Continuity	of the solution with respect to the boundary conditions Important because data do have errors $\Longrightarrow$ completely (*i.e.*, topologically) different solutions may be obtained using, *e.g.*, different instruments

Not well posed, not even for force-free BC

- $\downarrow$ Only one of the method (Grad-Rubin[1]) was proven to be a well-posed mathematical problem, at least for small nonlinearities.
- $\uparrow$ Multiple solutions to the 3D FF equations (either analytical or numerical) for a same set of BC have not been found yet

$\Longrightarrow$ Extrapolations techniques must be checked against known models, and, in applications, must be constrained by additional information

[1] Amari *et al*, AA **350** 1151 (1999)

Forget the photosphere ...

(... for the moment) and reformulate the problem as

- Find the (coronal) magnetic field in a numerical box for given conditions at the lower (photospheric) boundary, assuming a perfectly force-free field ... everywhere

- Discard: non-force-free effects close to the photosphere and errors in, or inconsistencies of, measured photospheric fields

Let's look at general properties and solution methods of the FF equations

Even in this extremely simplified formulation it is not a well-posed mathematical problem.

General properties of FFF

- Energy in the half-space can be computed using the virial theorem

The energy of the FF field in the half-space is (Molodensky Sol.Phys. 1974)

$$E = \int_{mgm} (xB_x + yB_y)\, B_z\, dxdy$$

However, if the BCs are not FF, then the energy depends on coordinates (see Wheatland & Metcalf ApJ 2006 for additional details)

- The components of the field at the boundaries are related to each other

Using $\vec{J} \times \vec{B} = \vec{\nabla} \cdot \vec{\vec{T}}$ where $\vec{\vec{T}} = (\vec{B}\vec{B} - \vec{\vec{I}}B^2/2)$, the Lorentz force in the volume above the mgm is (Molodenski Soviet Ast. 1969, Aly Sol.Phys. 1989)

$$\vec{\mathcal{F}} = \int_{\mathcal{V}} \vec{\nabla} \cdot \vec{\vec{T}} \mathrm{d}\mathcal{V} = \oint_{\partial\mathcal{V}} \vec{\vec{T}} \cdot \mathrm{d}\vec{S}$$

or, in components,

$$\mathcal{F}_x = -\int_{mgm} B_x B_z\, dxdy \qquad \mathcal{F}_y = -\int_{mgm} B_y B_z\, dxdy \qquad \mathcal{F}_z = \frac{1}{2}\int_{mgm} (B_x^2 + B_x^2 - B_z^2)\, dxdy$$

and similar for the torque $\int_{\mathcal{V}} \vec{r} \times \vec{\nabla} \cdot \vec{\vec{T}}$. The second line holds if the mgm is flux balanced.

- Field components on mgm $\Longrightarrow$ the knowledge of the field inside $\mathcal{V}$ is not required
- Sort of “sufficient” definition of what a “FF-compatible” boundary is: they should be small compared *e.g.*, with the magnetic pressure force $\frac{1}{2}\int_{mgm}(B_x^2 + B_x^2 + B_z^2)\, dxdy$

UCL MSSL

Two FFFs

The vanishing of the Lorentz force $\vec{J} \times \vec{B}$ can be satisfied by

- $\vec{J} = \vec{\nabla} \times \vec{B} = 0 \Longrightarrow$ potential field $B = \vec{\nabla}\phi$. Using $\vec{\nabla} \cdot \vec{B} = 0$

$$\begin{cases} \Delta\phi = 0\,, \\ \partial_n \phi|_{\mathcal{V}} = \hat{n} \cdot \vec{B}|_{\mathcal{V}} \end{cases}$$

  Only $\hat{n} \cdot \vec{B}|_{\mathcal{V}}$ is required to fully specify the solution (recall Thomson theorem)

- $\vec{J} \parallel \vec{B} \Longrightarrow$ typically a scalar function $\alpha(\vec{x})$ is introduced such that $\vec{J} = \alpha\vec{B}$,

$$\begin{cases} \vec{\nabla} \times \vec{B} = \alpha\vec{B} \\ \vec{B} \cdot \vec{\nabla}\alpha = 0 \end{cases}$$

  where the second relation is obtained from $\vec{\nabla} \cdot (\vec{J} = \alpha\vec{B})$ using $\vec{\nabla} \cdot \vec{B} = 0$

  - The first equation implies $\vec{J} \times \vec{B} = 0$
  - Fl of $\vec{J}$ coincide with fl of $\vec{B}$ (trivial, but useful for visualization)
  - α is constant along individual field lines, but changes from fl to fl

UCL MSSL

Potential fields

- PF as current-free solution ($\alpha = 0$) of the NLFFF equations
- Unique solution with a well defined energy
- Often a good approximation of the large-scale topology
- Currents modify the topology, but large scale topological features (like QSLs) do not disappear (see *e.g.*, Aulanier *et al.*, A&A 2005)

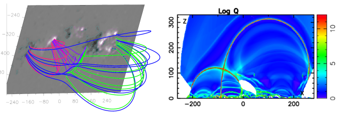

PF and QSL vertical cut (vanDriel *et al.*, ApJ 2014)

$\Longrightarrow$ Depending on the question, the PF may already provide the answer

The PF equation

$$\begin{cases} \Delta\phi = 0\,, \\ \partial_n \phi|_{\mathcal{V}} = \hat{n}\cdot\vec{B}|_{\mathcal{V}} \end{cases}$$

can be solved using the FT solution of the LFFF problem with $\alpha = 0$, which inherits the periodicity of the solution

Alternatively, for a flux balanced, isolated AR in a finite volume

- Use Green function solution only to fill in boundaries (Schmidt Proc-1964-Hess. 1964), where field is zero outside the FoV

$$\phi(x,y,z) = \frac{1}{2\pi}\int_{\text{photo}} \frac{B_z(x',y',z=0)}{\left((x-x')^2+(y-y')^2+z^2\right)^{1/2}}\, d\text{xdy}$$

- Use optimized Poisson solvers with the computed Neumann BC

But it is only the minimal energy state ...

The α parameter

α couples the elliptic part to the hyperbolic part of the problem

$$\begin{cases} \vec{\nabla} \times \vec{B} = \alpha \vec{B} & \text{elliptic, determines } \vec{B} \text{ from } \vec{J} \text{ distribution (\textit{i.e.}, from } \alpha) \\ \vec{B} \cdot \vec{\nabla} \alpha = 0 & \text{hyperbolic, propagates } \alpha \text{ (\textit{i.e.}, } \vec{J}) \text{ along the fl of a given connectivity} \end{cases}$$

- α is constant along individual field lines. If the magnetic vector field at $z = 0$ is known $\Longrightarrow$ the map of α at the photosphere

$$\alpha(x, y, z = 0) = \left. \frac{J_z}{B_z} \right|_{z=0} = \left. \frac{\partial_x B_y - \partial_y B_x}{B_z} \right|_{z=0}$$

  propagates upwards in the volume along field lines
- Therefore, the α at the two ends of a fl is the same $\Longrightarrow$ α on one polarity is sufficient
- Only B_z and the map of α on one polarity at the boundaries are required to fully specify the solution

- Geometrically, α is the local torsion of field lines, $\alpha = \hat{b} \cdot \vec{\nabla} \times \hat{b}$, with $\hat{b} = \vec{B}/|\vec{B}|$
- For a sheared arcade with $B \sim e^{-z/l_z}$ the shear $\tan(B_y/B_x)|_{z=0} = \alpha l_z$
- For a semi-circular twisted flux tube $\alpha 8H/(L\Phi^2)$, helicity per unit length and flux
- Typical AR average values of $|\alpha|$ range from 0 to 0.05 Mm^{-1} (Longcope *et al.*, ApJ 1998)

2. Linear force-free extrapolation

The linear approximation

Introduce the torsion scalar function $\alpha(\vec{x})$ such that $\vec{J} = \alpha\vec{B}$ and

$$\begin{cases} \vec{J} \times \vec{B} = 0 \\ \vec{\nabla} \cdot \vec{B} = 0 \end{cases} \Longrightarrow \begin{cases} \vec{\nabla} \times \vec{B} = \alpha\vec{B} \\ \vec{B} \cdot \vec{\nabla}\alpha = 0 \end{cases}$$

A simple way to satisfy $\vec{B} \cdot \vec{\nabla}\alpha = 0$ is to assume

$$\boxed{\alpha = \text{constant}}$$

- $\vec{\nabla} \times \vec{B} = \alpha\vec{B}$ becomes linear in $\vec{B}$ (LFFF) $\Longrightarrow$ solution by superposition, *e.g.*, Fourier
- Equivalently, taking $\vec{\nabla} \times (\vec{\nabla} \times \vec{B} = \alpha\vec{B})$ yields $\Delta\vec{B} + \alpha^2\vec{B} = 0$ an Helmholtz equation for the three components separately, linear in $\vec{B}$
  In this case $\vec{\nabla} \cdot \vec{B} = 0$ must be imposed explicitly by $\vec{B} = \vec{\nabla} \times \vec{A}$, and the gauge condition reduces the problem to the solution of a scalar Helmholtz equation

- Analytical solutions are known which give $\vec{B}$ in $\mathcal{V}$ as a function of its values on $\partial\mathcal{V}$
  - Green functions: Chiu & Hilton ApJ 1997; Seehafer SP 1978
  - Fourier: Nakagawa & Radu SP 1972; Alissandrakis A&A 1981
  - Spherical harmonics: Newkirk 1969
  - Superposition of discrete sources: Lothian & Browning SP 1995
  - Reviews: Sakurai SP 1981, Wiegelmann & Sakurai LRSP 2013
- Under conditions, only $\hat{n} \cdot \vec{B}|_{\partial\mathcal{V}}$ is required to fully specify the solution $\Longrightarrow$ LoS mgm as BC
- By normalizing lengths, α can be eliminated from the equations $\Longrightarrow$ BCs cannot fix it

$$\boxed{\alpha \text{ is a free parameter}}$$

Alissandrakis' solution

On the computation of constant alpha force-free magnetic field
C.E. Alissandrakis, Astronomy and Astrophysics, **100**, 1, July 1981, p. 197

- Variable separation in z and Fourier expansion in (x, y): $\vec{B}(x, y, z) \xrightarrow[(u,v)]{\text{FT}} \vec{b}(u, v)\exp(-kz)$
- Substitute in $\vec{\nabla} \times \vec{B} = \alpha\vec{B} \Longrightarrow$ system of linear eqs., the solution exists if $k = \pm\sqrt{(4\pi^2(u^2 + v^2) - \alpha^2)}$
- The magnetic field is then given in terms of the FT of the observed magnetogram, $b_z(u, v, z = 0)$ as

$$\vec{B}(x, y, z) = (FT)^{-1}\left(\vec{G}(u, v, z)b_z(u, v, 0)\right)$$

Two contributing solutions

- "Small scale solution" where k is real: $|\alpha| \leq 2\pi(u^2 + v^2)^{1/2}$

$$\hat{G}_x(u, v, z) = -i\frac{uk - v\alpha}{2\pi(u^2 + v^2)}e^{-z(4\pi^2(u^2+v^2)-\alpha^2)^{1/2}}$$

and similar for the other components (equivalent to Nakagawa & Radu Sol.Phys. 1972)

- "Large scale solution" where k is imaginary: $|\alpha| > 2\pi(u^2 + v^2)^{1/2}$

$$\hat{G}_x(u, v, z) = \hat{G}_x\left(u, v, \gamma, \sin/\cos((\gamma z))\right), \qquad \text{with } \gamma = (\alpha^2 - 4\pi^2(u^2 + v^2))^{1/2}$$

with oscillating terms in $z \Longrightarrow$ diverging energy, and requires the knowledge of B_x and B_y at $z = 0$ (equivalent to the Green method in Chiu & Hilton ApJ 1997)

- $|\alpha| \leq \alpha_{\max} = \min\left(\frac{2\pi}{L_x}, \frac{2\pi}{L_y}\right)$ Limit on $\alpha_{\max}$, *i.e.*, on $\vec{J}$, derives from the size of the FoV, not from the structure of $\vec{B}$

Fast, accurate and easy to implement

UCL MSSL

Constrains to α

In order to have

- finite energy in the column above the mgm of extension (L_x, L_y)
- unique solution

the Fourier coefficients $\vec{b}(u, v, z=0) \neq 0$ only at discrete wavenumbers

$\Longrightarrow$ periodic repetition (without DC component, *i.e.*, mgm is flux balanced)

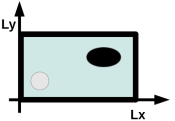

The field is flux balanced ($\vec{b}(0,0) = 0$) $\Longrightarrow$ the periodically repeat the mgm (L_x, L_y), imposing that $|\alpha|$ is smaller than the smallest eigenvalue yields

$$|\alpha| \leq \alpha_{\max} = \min\left(\frac{2\pi}{L_x}, \frac{2\pi}{L_y}\right)$$

(Nakagawa & Radu Sol.Phys. 1972; Chiu & Hilton ApJ 1997; Alissandrakis A&A 1981)

A DC component gives fl extending to infinity

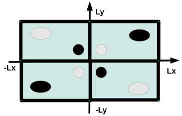

The field is not flux balanced: the combination of the original mgm with its the three point-mirror images is flux balanced, which yields a slightly modified condition

$$|\alpha| \leq \alpha_{\max} = \min\left(\pi\left(\frac{m^2}{L_x^2} + \frac{n^2}{L_y^2}\right)^{1/2}\right)$$

with $m, n = 1, 2\ldots$

(Seehafer Sol.Phys. 1978)

Effective double domain in x and y

For $L_x = L_y$, the difference between the two $\alpha_{\max}$ is a factor $\sqrt{2}/2$, a factor $\sqrt{5}/2$ if the mgm is flux balanced

Limit on $\alpha_{\max}$, *i.e.*, on $\vec{J}$, is unphysical: derives from the size of the FoV, not from the structure of $\vec{B}$

UCL MSSL

Tips and tricks

- As a rule, Green functions methods are slower than Fourier solutions (FFT)
  For a plane, Green methods require N^4 operations, FFT require $(N \log_2 N)^2$ operations
- The field at the photosphere is known on a grid $\Longrightarrow$ DFT/FFT is affected by aliasing. Typically, this he effect is reduced by padding the mgm with zeros (which, however, lower even more $\alpha_{\max}$)
- The sign of α in AR can be guessed (tongues, chirality of fls, sigmoids) $\Longrightarrow$ Fourier methods can be implemented for only positive (respectively, only negative) values of α mapping into the $(0, 2\pi)$ (respectively, $(-2\pi, 0)$) frequency interval, rather than in $(-\pi, \pi)$, which doubles the value of $\alpha_{\max}$

UCL MSSL

How to fix α

<u>Best-α method</u> (Petsov *et al.*, ApJ 1995). Choose the α value that minimize the residual $\mathcal{R}$

$$\mathcal{R}(\alpha, B_{\text{thr}}) = \sum_{|B_z|>B_{\text{thr}}} \left((B_{\text{x,LFFF}} - B_{\text{x,mgm}})^2 + (B_{\text{y,LFFF}} - B_{\text{y,mgm}})^2 \right)^{1/2}$$

For each α in the $|\alpha| \leq \alpha_{\text{max}}$ only the computation the LFFF at $z = 0$ is necessary.

Simple, fast, and elegant, but it requires the knowledge of the vector mgm

<u>Comparing fl with EUV or SXR loops in 2D</u>

Iteratively finds the value of α that minimize the distance between extrapolated and EUV/SXR loops, in average sense

(Green *et al.*, Sol.Phys. 2002, Carcedo *et al.*, Sol.Phys. 2003, Feng *et al.*, ApJ 2007).

- It can be always applied (EUV and SXR images are taken more often than mgm)
- Still, it employs 2D projection of 3D structures.
- Human factor in identifying loops, moreover loops ends not always visible (help from automated feature recognition methods, *e.g.*, Inhester *et al.*, Sol.Phys. 2008)

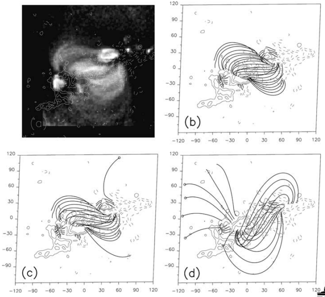

(a) Yohkoh/SXT (b) $\alpha = -1.26 \times 10^{-2}$ Mm^{-1}, best-fitting case; (c) Slightly worse matching ($\alpha = -1.51 \times 10^{-2}$ Mm^{-1}); (d) Wrong sign of α (Green *et al.*, Sol.Phys. 2002)

Energy and helicity in LFFFs

In LFFF, free magnetic energy [$\mathcal{E}_c$], (relative magnetic) helicity [H_m], and α are explicitly related

General relations (Berger Astrophys. J. Suppl. 1985)

$$\mathcal{E}_c = \mathcal{F}\mathcal{E}_p$$

$$H_m = \frac{8\pi}{\alpha}\mathcal{F}\mathcal{E}_p$$

$$\mathcal{F} = \mathcal{F}\left(u, v, b_{u,v}, (u^2 + v^2 - d^2\alpha^2)\right)$$

α cannot be taken out of $\mathcal{F}$

d = linear size of the pixel, $\mathcal{E}_p$ = energy of the potential field

$$\mathcal{E}_p = \frac{1}{8\pi}\int_{z=0} \vec{z}\cdot(\vec{B}_p \times \vec{A}_p)\,\mathrm{d}x\mathrm{d}y$$

as surface integral (use *e.g.*, Alissandrakis' LFFF solution)

Linearized (in α) version (Démoulin *et al.*, A&A 2002, Georgoulis & LaBonte ApJ 2007)

$$\mathcal{E}_c = \mathcal{F}_l d^2\alpha^2\mathcal{E}_p\,,$$

$$H_m = 8\pi\mathcal{F}_l d^2\alpha\mathcal{E}_p$$

$$\mathcal{F}_l = \frac{1}{2}\frac{\sum_{u,v}|b_{u,v}|^2/(u^2+v^2)^{3/2}}{\sum_{u,v}|b_{u,v}|^2/(u^2+v^2)^{1/2}}$$

where $\mathcal{F}_l$ is independent of α

- The general formulae show the (unphysical) resonance at $\alpha = \alpha_{\max}$
- The linearized formulae
  - no resonance for a given $\alpha_{\max}$
  - almost overlap for different $\alpha_{\max}$

The linearized formulae represent a lower limit to (LFFF) $\mathcal{E}_c$ and H_m that can be prolonged beyond the nominal $\alpha_{\max}$

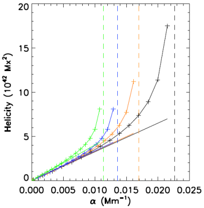

$H_m(\alpha)$ for different $\alpha_{\max}$ (vertical dashes). Solid lines= linearized formulae Crosses=general formulae

UCL MSSL

Evolution of α in time

An alternative way to fix alpha, in time (Valori *et al.*, Sol.Phys. 2015)

- The helicity flux through the photosphere can be measured using (vector or LoS) mgm (Pariat *et al.*, Astron. Astrophys. 2005)
- Estimate or assume $H_m(t = 0)$, *e.g.*, start before AR emergence
- The linearized formulae convert the measured $H_m(t)$ into $\alpha(t)$

$\Longrightarrow$ Time evolution of α, but without effect of CMEs

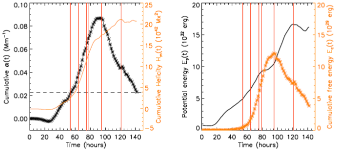

Left: Accumulated $\alpha(t)$ and $H_m(t)$ Right: Accumulated $\mathcal{E}_c(t)$ and $\mathcal{E}_p(t)$

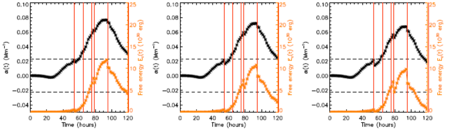

Renormalized $\alpha(t)$ and $\mathcal{E}_c(t)$ for 3 values of the free parameter

- Using GOES fluxes as proxy of the relative liberated energy in each event
- $\Delta\mathcal{E}_c \simeq H_m \Delta\alpha / 4\pi$
- Fixing the only free parameter (α at one particular time) using standard methods (*e.g.*, EUV)

$\Longrightarrow$ Time evolution of α with flare intensity scaling

UCL MSSL

Applications of LFFF methods

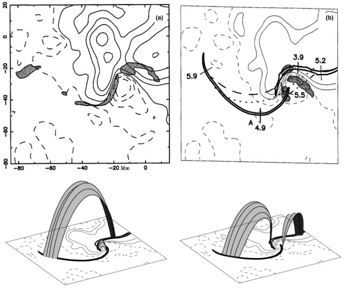

QSL rooted at observed ribbons position

Flare ribbons and QSLs

- QSLs from LFFF
- Location of QSL is found to match flare ribbons
- First proof of QSL role in coronal reconnection without nulls

Démoulin AdSpR 2006

AR outflows

- Outflow over monpolar areas, on QSL separaing closed from long/open fl
- Reconnection between hot and dense closed AR fls with cooler CH fls
- Contribution from AR boundaries to slow wind
- QSL from LFFF

Baker *et al.*, SP 2009

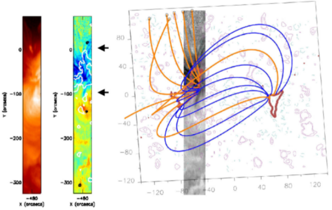

Outer and inner fl from a QSL at the AR boundary

Applications of LFFF methods

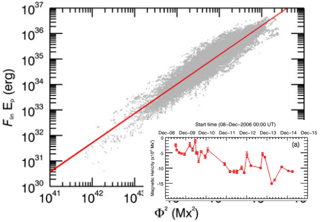

Scaled linear energy ad a function of flux for 56,686 ARs, and *H*

Connectivity-based method for the computation of *H*

- Collection of constant-α flux tubes
- Statistical approximation of the relation between scaled energy and flux
- Estimation of relative *H* based on magnetograms only

Georgoulis *et al.*, ApJ 2012

Time evolution of α

From Georgoulis *et al.*, ApJ 2007 combining

- time evolution of the helicity flux
- LFFF relation between *H* and *E*
- GOES fluxes to account for *E* and *H* depletions due to CMEs

derive $\alpha(t)$ (factor two smaller than coronal α)

Valori *et al.*, SP 2015

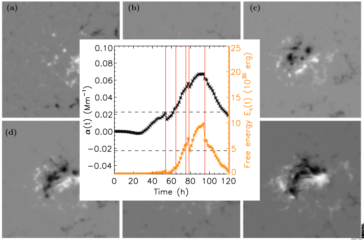

AR10365 time evolution of $\alpha = Jz/Bz$

UCL MSSL

LFFF: pros & cons

Depending on the question, the LFFF can provide the answer

Advantages

- Analytical solution in terms of observed quantities, *i.e.*, numerical implementations are simple and fast
- General relations can be derived
- Well-posed problem, under certain constrains
- Since only the LoS is required, huge historical database (*e.g.*, SOHO/MDI), nowadays at high time-cadence and resolution for full disk (SDO/HMI)

Drawbacks

- α is a global free parameter
- Cannot render potential and current-carrying at the same time
- Unphysical limitation on α
- Currents are mostly on large scales, which is not what is observed
- Similarly, H_m has an inverse cascade, hence in a relaxation to a LFFF $\Longrightarrow$ overestimation on large scale / underestimation on small scales (Démoulin *et al.*, A&A 2002)

LFFF mehtods are still used to produce relevant scientific results

UCL MSSL

Two counter-examples

The TD test case

- NLFFF: current ring surrounded by potential field, averaged twist: $\Phi = 1.4\pi$
- LFFF: $\alpha = \alpha_{\rm best} = 0.6$ (with $\alpha_{\rm max} = 0.8$)

No flux rope: The LFFF cannot render the real field topology.

NLFFF (top) and LFFF (bottom), 3D (left) and top (right) views (Valori *et al.*, A&A 2010)

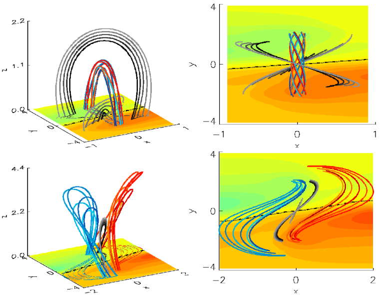

An AR case

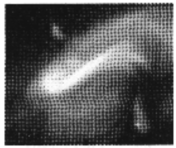

Figure 5. The Yohkoh SXT image of the Active Region NOAA 7912 on 14 Oct 1995 at 17:58:58 UT

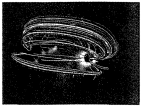

a- Linear force-free model

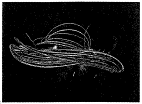

b- Non-linear force-free model

- LFFF $\alpha = 0.004$ Mm^{-1} (such that H_m is the same as NLFFF)
- NLFFF with GR method

The LFFF does not reproduce the curvature of SXR loops, even though H_m is the same

$\Longrightarrow$ $\vec{J}$ is not reproduced (hence not the free energy)

AR7912: Yokoh/SXT (left), LFFF (right, top) and NLFFF (right bottom) (Bleybel *et al.*, 9th EMSP 1999)

UCL MSSL

3. Nonlinear force-free extrapolation

Main methods overview

$$\begin{cases} \vec{J} \times \vec{B} = 0 \\ \vec{\nabla} \cdot \vec{B} = 0 \end{cases}$$

- Seek a current-carrying solutions in a finite volume
- No analytical solution in terms of (observed) boundary values is known
  $\Longrightarrow$ Numerical solution of the BVP

Different (more or less standard) approaches yield different methods

"Linearize" the nonlinearity (in α): **split the coupling** between elliptic and hyperbolic parts, and solve separately, then iteratively
$\Longrightarrow$ Grad-Rubin

Introduce a **global functional** of $\vec{B}$ that is minimized if $\vec{B}$ is FF, then find its minimum as a pseudo-time evolution
$\Longrightarrow$ Optimization

Direct solution: Use Green identities to relate values of $\vec{B}$ on the boundary to values of $\vec{B}$ in the volume, projecting on a set of **trial solutions** with coefficients to be determined iteratively
$\Longrightarrow$ Boundary Integral

Numerical relaxation: Solve the **IVP** that has the BVP as solution at $t \to \infty$, as a pseudo-time evolution
$\Longrightarrow$ Magneto-frictional

All methods would lead to the same solution if the corresponding BVPs were well-posed ...

These are the most used / currently developed / extensively tested methods. For more details see references in reviews:
Wiegelmann JGR 2008, Wiegelmann & Sakurai LRSP 2013, Regnier Sol.Phys. 2013

Grad-Rubin method

Solve the system of linear equations

$$\begin{cases} \vec{B}^{[k]} \cdot \vec{\nabla}\alpha^{[k]} = 0 \\ \vec{\nabla} \times \vec{B}^{[k+1]} = \alpha^{[k]}\vec{B}^{[k]} \end{cases}$$

where k is an iteration index

At each iteration k

- for the given $\vec{B}^{[k]}$, propagate α along field lines (hyperbolic part) $\Longrightarrow$ requires α on one polarity
- for a given current distribution $\alpha^{[k]}\vec{B}^{[k]}$, solve the Biot-Savart (elliptic) part to get $\vec{B}^{[k+1]}$ $\Longrightarrow$ requires $\hat{n} \cdot \vec{B}|_{\partial\mathcal{V}}$
- The iteration starts with the potential field, $\vec{B}^{[k=0]}$, and ends when an iteration fixed point is reached
- The $\vec{B}^{[k]}$ at the fixed point of the iteration is a solution to the FF equation

In implementations of the GR (see *e.g.*, Wheatland Sol.Phys. 2007) typically

- The hyperbolic part is solved by ray-tracing methods (trace field lines from any grid point to the bottom boundary)
- The vector potential representation is used to insure the solenoidal property, and the Poisson problem associated to the elliptic part is solved using Fourier decomposition (but see Amari A&A 2006 and Inhester & Wiegelmann Sol.Phys. 2006 for alternative methods)
- Both periodic and nonperiodic BC have been implemented

- Well posed problem in finite domain, for small α (Amari *et al.*, A&A 2006). Numerical convergence might be an issue
- There are two extrapolations for each mgm: the positive (negative) solution given by specifying α on $B_n > 0$ ($B_n < 0$). Recently, Wheatland *et al.*, ApJL 2011 and Amari & Aly A&A 2010 proposed iterative methods for merging of the two solutions
- α is “instantaneously” propagated along the whole field line in the volume, at each iteration
- α is derived from the observation by, *e.g.*, finite differences, which amplify the noise of observed data
- Spherical version of the method have been developed (see *e.g.*, Amari *et al.*, A&A 2013)

UCL MSSL

Optimization method

- $L = \int_{\mathcal{V}} \left(\frac{|\vec{J} \times \vec{B}|^2}{|B|^2} + |\vec{\nabla} \cdot \vec{B}|^2 \right) \mathrm{d}\mathcal{V}$, positive, vanishes if $\vec{B}$ is FF
- Take the functional derivative of L, a pseudo-time evolution for $\vec{B}$ is found

$$\frac{\partial \vec{B}}{\partial t} = \mu \vec{F} \qquad \text{such that} \qquad \frac{1}{2}\frac{dL}{dt} = -\int_{\mathcal{V}} \mu F^2 \mathrm{d}\mathcal{V}$$

i.e., such that L is decreasing in time (if $\partial_t \vec{B}|_{\partial\mathcal{V}} \neq 0$ there is $\int_{\partial\mathcal{V}}$)

$$\mathbf{F} = \nabla \times \left(\frac{[(\nabla \times \mathbf{B}) \times \mathbf{B}] \times \mathbf{B}}{B^2} \right) + \left\{ -\nabla \times \left(\frac{((\nabla \cdot \mathbf{B})\mathbf{B}) \times \mathbf{B}}{B^2} \right) - \Omega \times (\nabla \times \mathbf{B}) - \nabla(\Omega \cdot \mathbf{B}) + \Omega(\nabla \cdot \mathbf{B}) + \Omega^2 \mathbf{B} \right\} \qquad (30)$$

- μ is an arbitrary positive function and

$$\Omega = \mathbf{B}^{-2}[(\nabla \times \mathbf{B}) \times \mathbf{B} - (\nabla \cdot \mathbf{B})\mathbf{B}]. \qquad (31)$$

- The initial field is (usually) the potential field with the transverse observed components overwritten (which makes $L \neq 0$)
  $\Longrightarrow$ requires the three components of the field at the photospheric boundary
- Evolve the magnetic field according to the pseudo-time evolution equation
- Checks on L values for step acceptance, yielding monotonic decrease of L
- The evolution is stopped when L is below a given threshold (or not decreasing any longer)

In the implementations of the OM

- The $\partial_t \vec{B}|_{\partial\mathcal{V}} = 0$ is relaxed using a weighting function in L (buffer) to reduce the effect of lateral and top boundaries (Wiegelmann Sol.Phys. 2004)
- Finite differences (Wheatland *et al.*, 2000, Wiegelmann Sol.Phys. 2004) and finite element (Inhester & Wiegelmann Sol.Phys. 2006) discretizations
- Very flexible method: many additional constrains have been inplemented, *e.g.*, a term is added in L that allows for deviations from observed data where large errors are present at the bottom boundary (Wiegelmann & Inhester A&A 2010)

- Three boundary conditions are necessary for the OM (whereas the FF problem is defined by two)
- Inconsistent BC will in general produce solutions that are neither solenoidal nor FF
- No α propagation as in GR, the injection of parallel currents depends on coupling with the bottom boundary $\Longrightarrow$ multi-gridding techniques
- A spherical version of the method was developed (see Wiegelmann *et al.*, A&A 2007)

UCL MSSL

Magneto-frictional method

Relaxation technique: the BVP

$$\begin{cases} \vec{\nabla} \times \vec{J}_\perp = 0 \\ \vec{\nabla} \cdot \vec{B} = 0 \end{cases}$$

is the $t \to \infty$ solution of the IVP

$$\frac{1}{\nu}\frac{\partial \vec{B}}{\partial t} = -\vec{\nabla} \times \vec{J}_\perp + \vec{\nabla}(\vec{\nabla} \cdot \vec{B})$$

- Does not solve the FF, but a FF solution is obtained if the BC are FF
- Diffusive equation (Craig & Sneyd ApJ 1986) for $\vec{J}_\perp$ and $\vec{\nabla} \cdot \vec{B}$

$$\frac{1}{\nu}\frac{\partial E_M}{\partial t} = -\int_{\mathcal{V}} dV \, (J_\perp^2 + (\vec{\nabla} \cdot \vec{B})^2)$$

  a static state is reached where the solution is FF and DF
- The initial field is the potential field with the transverse observed components overwritten (which makes $\vec{J}_\perp$ and $\vec{\nabla} \cdot \vec{B} \neq 0$) $\Longrightarrow$ requires the three components of the field at the photospheric boundary
- Evolve the magnetic field according to the pseudo-time evolution equation, until a static state is reached

In the implementations of the MF

- 4^{th} CD in space, Runge-Kutta-Chebyscev in time (Valori *et al.*, A&A 2010), several BC (Valori *et al.*, Sol.Phys.2007)
- For an implementation of the MF method using the CESE-MHD code see Jiang & Feng ApJ 2012

- Slow but very robust due to diffusive nature
- Three boundary conditions are necessary for the OM (whereas the FF problem is defined by two)
- Inconsistent BC will in general produce solutions that are neither solenoidal nor FF. However, explicit relation between nonFF of the boundary to the nonFF of the solution:
  $\int_{\mathrm{mgm}} \hat{\hat{z}} \cdot (\vec{J}_\perp \times \vec{B} - (\vec{\nabla} \cdot \vec{B})\vec{B}) dxdy = \int_{\mathcal{V}} dV \, (J_\perp^2 + (\vec{\nabla} \cdot \vec{B})^2)$
- No α propagation as in GR, the injection of parallel currents depends on coupling with the bottom boundary $\Longrightarrow$ multi-gridding techniques
- MF is related OM and was derived as a dominant-viscosity case of MHD (Yang *et al.*, ApJ 1987)
- A spherical version of the method was developed (Y. Guo *et al.*, , ApJ 2007)

UCL MSSL

Boundary element method

From the 2[nd] Green identity

$$\vec{B}(\vec{x}) = \int_{\partial\mathcal{V}} \left(\vec{Y}\frac{\partial \vec{B}}{\partial n} - \vec{B}(z=0)\frac{\partial \vec{Y}}{\partial n} \right) \mathrm{d}\mathcal{V}$$

where the λ_i in $Y_i = \cos(\lambda_i r)/4\pi r$ must satisfy

$$\int_{\mathcal{V}} Y_i \left(\lambda_i^2 B_i - \alpha^2 B_i - (\vec{\nabla}\alpha \times \vec{B})_i \right) = 0$$

- It is a direct solution in terms of observed values, but not a closed one due to λ_i
- As a Green method, the field in one point requires one surface integral, but the determination of λ_i require an additional volume integral $\Longrightarrow$ inherently slow

In the implementations of the BI

- An iterative procedure for fixing λ_i was introduced (DBIE, Yan & Li, ApJ 2006)
- Recent application to SDO/HMI data (Wang *et al.*, arXiv:1306.1122) using GPU tecniques

- Pointwise solution of the FF
- Both the full vector and α on the bottom boundary are necessary
- Published tests seems to perform comparably to (possibly slightly worse than) other methods
- The method seems to be intrinsically slow, and to require special tecnhiques in order to be used with high resolution mgm.

Other methods

MHD evolutionary methods

Use some approximation of the zero-β MHD under

$$\partial_t \rho = -\nabla \cdot (\rho\, u),$$
$$\rho\, \partial_t u = -\rho\,(u \cdot \nabla)\, u + j \times B + \nabla \cdot \mathrm{T},$$
$$\partial_t B = \nabla \times (u \times B),$$

1. Strong viscosity in $\vec{\nabla} \cdot \vec{T}$
2. Phtospheric driving reproducing the mgm

- $\vec{\nabla} \cdot \vec{B}$ cleaner Inoue *et al.*, , ApJ 2014
- CESE-MHD NLFFF CODE Jiang and Feng, ApJ 2013

Vertical Integration Method

The FF equations can be written as

$$\partial_z B_x = \partial_x B_z + \alpha B_y$$
$$\partial_z B_y = \partial_y B_z - \alpha B_x$$
$$\partial_z B_z = -\partial_x B_x - \partial_y B_y$$
$$\partial_z \alpha = (-B_x \partial_x \alpha - B_y \partial_y \alpha)/B_z$$

- $\vec{B}(z + \Delta z)$ is determined by direct integration from $\vec{B}(z)$, similar to an IVP with $z = t$
- Ill-posed: no BC can be imposed at the 'top' $\Longrightarrow$ any error is exponentially amplified with height
- Singularity at $B_z = 0$ must be treated
- Many failed attempt to regularize the solution (see *e.g.*, Demoulin *et al.*, Sol.Phys. 1997, Amari *et al.*, A&A 1998)

UCL MSSL

Main methods overview

Grad-Rubin

$$\begin{cases} \vec{\nabla} \times \vec{B} = \alpha \vec{B} \\ \vec{B} \cdot \vec{\nabla}\alpha = 0 \end{cases} \Longrightarrow \begin{cases} \vec{\nabla} \times \vec{B}^{[k+1]} = \alpha^{[k]} \vec{B}^{[k]} \\ \vec{B}^{[k]} \cdot \vec{\nabla}\alpha^{[k]} = 0 \end{cases}$$

- Linearize by splitting elliptic and hyperbolic part
- if converge to the same solution then $\vec{B}$ is FF
- BC: B_n and α on one polarity

Optimization

$$\begin{cases} \vec{J} \times \vec{B} = 0\,, \\ \vec{\nabla} \cdot \vec{B} = 0 \end{cases} \Longrightarrow L = \int_{\mathcal{V}} \frac{|\vec{J} \times \vec{B}|^2}{|B|^2} + |\vec{\nabla} \cdot \vec{B}|^2 \mathrm{d}\mathcal{V}$$

- if $L = 0$ then $\vec{B}$ is FF
- Prescribe $\partial_t \vec{B}$ such that L is minimized
- BC: Three components are prescribed

Boundary Integral

$$\begin{cases} \vec{\nabla} \times \vec{B} = \alpha \vec{B} \\ \vec{\nabla} \cdot \vec{B} = 0 \end{cases} \Rightarrow \begin{cases} c_i \vec{B}_i = \int_{\partial\mathcal{V}} \left(\vec{Y} \frac{\partial \vec{B}}{\partial n} - \frac{\partial \vec{Y}}{\partial n} \vec{B}_0 \right) \mathrm{d}\vec{S} \\ Y_i = \frac{\cos(\lambda_i r)}{4\pi r}\,, \quad i = x, y, z \end{cases}$$

- Use Green identities to relate $\vec{B}$ in $\mathcal{V}$ to $\vec{B}(z=0) = \vec{B}_0$
- λ_i are determined iteratively
- BC: Three components and α are prescribed

Magneto-frictional

$$\begin{cases} \vec{\nabla} \times \vec{J}_\perp = 0\,, \\ \vec{\nabla} \cdot \vec{B} = 0 \end{cases} \Longrightarrow \partial_t \vec{B} = -\vec{\nabla} \times \vec{J}_\perp + \vec{\nabla}(\vec{\nabla} \cdot \vec{B})$$

- Consider an IVB for $\vec{B}$, diffusion of $\vec{J}_\perp$ and $\vec{\nabla} \cdot \vec{B}$
- if a static state is reached then $\vec{B}$ is FF
- BC: Three components are prescribed

- All iterative methods, often use the PF as initial state of an iterative/pseudo-time evolution
- Each method **use the BC differently** (directly on in some combination, *e.g.*, $\alpha = J_z/B_z$)
- They basically solve **different problems**, possibly equivalent if the BC are FF (but no proof)

Quite likely to get different solutions if BC are non-FF

UCL MSSL

Does it happen?

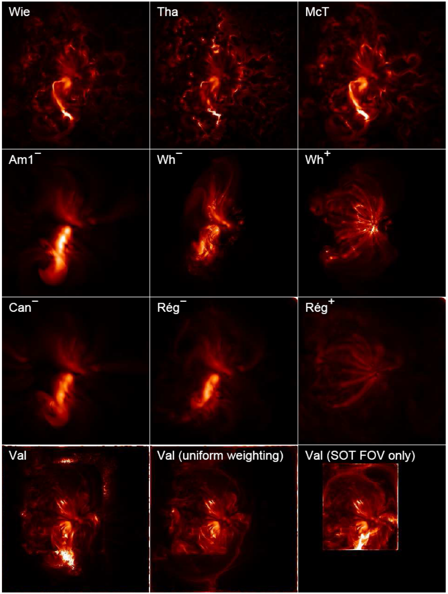

Integrated los $|\vec{J}|$ of AR10953 for different extrapolation codes

Same magnetogram, different methods.

Note that, in this case, the largest differences are to be found between P and N solutions of GR methods

More than 60 (!) extrapolations were analysed in a NLFFF-Consortium comparative paper that differs in methods, implementations, bc, mgm preprocessing, embedding.

DeRosa *et al* ApJ **696** 280 (2009)

Different methods react differently to the inconsistency between the FF assumption and magnetogram

UCL MSSL

Twisted coronal structures

- Kink and torus instabilities as driver of eruptions
  Török, Kliem, ApJ, **630**, L97 (2005)
  Kliem and Török Phys. Rev. Lett. **96** (2006)
- Twisted structures enter all CME initation models

⟹ Extrapolation should accurately reproduce twist.

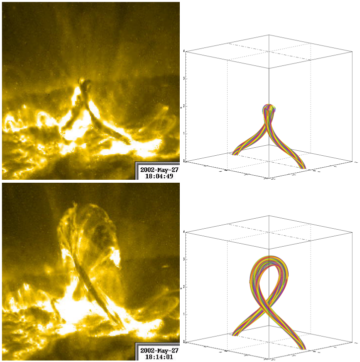

TRACE images of a flaring region and the corresponding numerical simulation of a kink-unstable flux rope

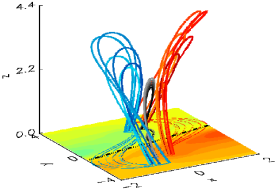

We have seen how the LFFF fails with TD. Is NLFFF any better?

UCL MSSL

Test case of a flux rope: TD

Titov and Démoulin[2]: 3D solution of the nonlinear, force-free equations consisting of a current ring surrounded by a potential field.

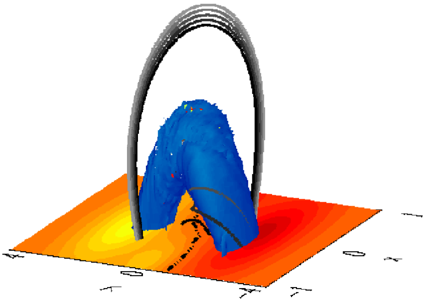

TD: Current density iso-surface at 30% of peak

Equilibrium is insured by a balance between the current ring self-force and the external poloidal field generated by two subphotosperic magnetic charges. In this application, two buried magnetic dipoles fix the average twist to -2.12π.

The field rapidly decreases away from the flux rope.

TD models a compact, bipolar AR, with two satellite sunspots connected by a current-carrying flux rope.

[2] Titov and Démoulin, A&A **351** 707 (1999)

Test case of a flux rope: TD

Titov and Démoulin[2]: 3D solution of the nonlinear, force-free equations consisting of a current ring surrounded by a potential field.

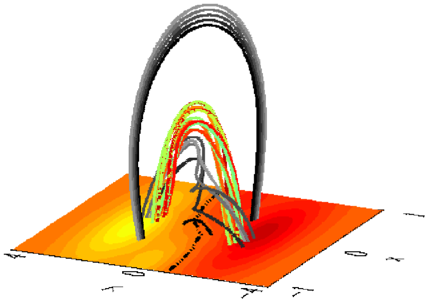

TD: Field lines

Equilibrium is insured by a balance between the current ring self-force and the external poloidal field generated by two subphotosperic magnetic charges. In this application, two buried magnetic dipoles fix the average twist to -2.12π.

The field rapidly decreases away from the flux rope.

TD models a compact, bipolar AR, with two satellite sunspots connected by a current-carrying flux rope.

[2] Titov and Démoulin, A&A **351** 707 (1999)

TD: extrapolation results

Only the vector field at the bottom is used as input. Small errors on[3]

- Solution consistency
  - $\sigma_J = 0.007$
  - $< |f_i| >= 7 \times 10^{-5}$
- Morphology
  - 0.6% apex CFL
  - 0.5% apex HFT
- Stability and energy
  - 1.1% twist
  - 4.4% helicity
  - 0.4% energy

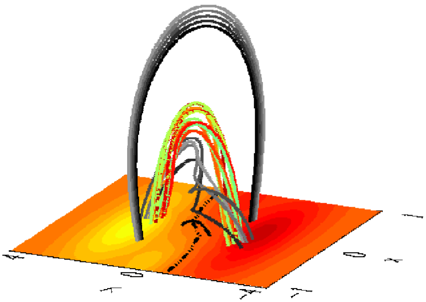

TD equilibrium field

σ_J=CWsin θ= current-averaged sine angle between $\vec{B}$ and $\vec{J} = (\int dV\, |\vec{J}_\perp|) / \int dV\, |\vec{J}|$

$f_i \equiv (\int_{v_i} dv_i \vec{\nabla} \cdot \vec{B}) / \int_{\partial v_i} ds_i |vB|$ fractional flux generated in v_i

$\Longrightarrow$ The MF method reconstructs the TD with great accuracy

[3] Valori, Kliem, Török, Titov, A&A **519** A44+ (2010)

TD: extrapolation results

Only the vector field at the bottom is used as input. Small errors on[3]

- Solution consistency
  - $\sigma_J = 0.007$
  - $< |f_i| >= 7 \times 10^{-5}$
- Morphology
  - 0.6% apex CFL
  - 0.5% apex HFT
- Stability and energy
  - 1.1% twist
  - 4.4% helicity
  - 0.4% energy

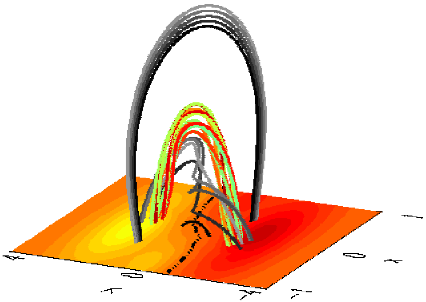

TD: Reconstructed field

σ_J=CWsin θ= current-averaged sine angle between $\vec{B}$ and $\vec{J} = (\int dV\ |\vec{J}_\perp|)/\int dV\ |\vec{J}|$

$f_i \equiv (\int_{v_i} dv_i \vec{\nabla}\cdot\vec{B})/\int_{\partial v_i} ds_i |vB|$ fractional flux generated in v_i

$\Longrightarrow$ The MF method reconstructs the TD with great accuracy

[3] Valori, Kliem, Török, Titov, A&A **519** A44+ (2010)

TD: HFT and BP reconstruction

The MF code can accurately reproduce complex topological features[3]

Hyberbolic Flux Tubes:

sort of 3D X-lines, preferred locations where current sheets are formed

Field lines are in grey if below the HFT, in green if above the HFT

Bald patches:

locations of inverse crossing of the B_z-pil by the poloidal component

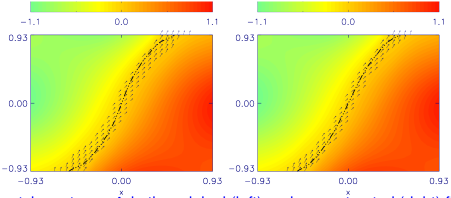

Bald patches at $z = \Delta$ in the original (left) and reconstructed (right) fields

$\Longrightarrow$ Topological features do not hinder extrapolation.

[3] Valori, Kliem, Török, Titov, A&A **519** A44+ (2010)

Strongly flux-unbalanced mgm

Half TD: flux unbalanced and current ring through the side boundary

Full mgm | Half mgm

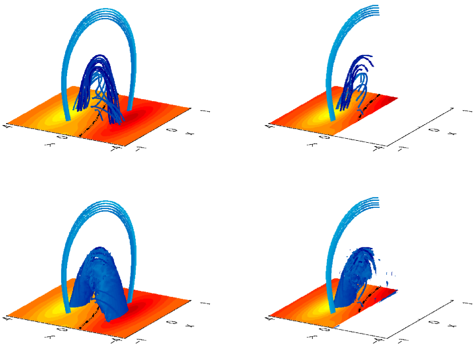

Field lines (top) and current density iso-surface at 33% of peak (bottom)

$\Longrightarrow$ MF code can handle current-carrying field lines leaving the box through non-photospheric boundaries.

Kink-unstable case

Initial and final configurations are (approximately) force-free states with the same vector magnetogram at the bottom.

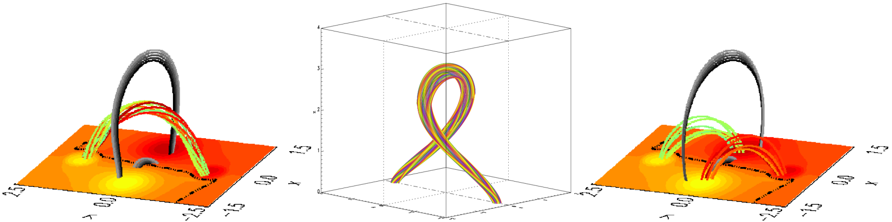

Initial, erupting, and final configurations of the unstable MHD evolution

What is the MF code producing in an unstable case[3]?

Much longer extrapolation run, with two clearly distinguished states of minimal and maximal energy/σ_J.

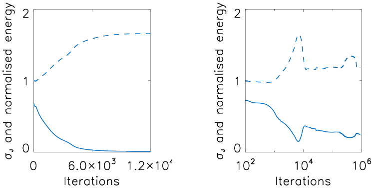

σ_J (solid) and energy (dashes) evolution in a stable (left) and unstable (right, logscale) cases.

3 Valori, Kliem, Török, Titov, A&A **519** A44+ (2010)

Kink-unstable case

The maximal and minimal energy/σ_J states correspond to different topological solutions:

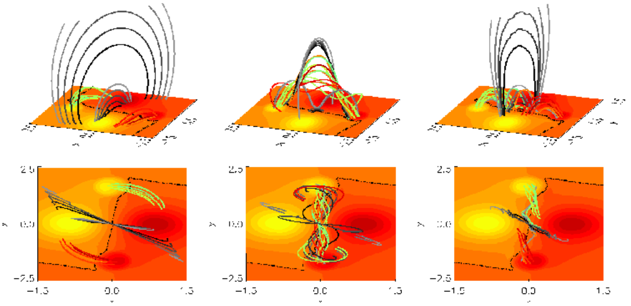

Initial (left), maximal energy (middle), and final (right) configurations of the extrapolated unstable case.

A flux rope is formed (at max energy/min σ_J) but rapidly destroyed. The final state of extrapolation is similar to the final state of the MHD eruption[3].

$\Longrightarrow$ Clear indication of the unstable carachter of the test field.

[3] Valori, Kliem, Török, A&A **519** A44+ (2010)

Test conclusions

The MF nonlinear extrapolation method, when confronted with a force-free compatible boundary like the TD,

- can reconstruct the 3D, force-free magnetic field with very high accuracy
- is not hindered by topological complexity (*e.g.*, fl with more than one turn, BP, HFT)
- does not require flux balance in the input mgm (open sides and top)
- can indicate if the vector mgm corresponds to an unstable configuration

$\Longrightarrow$ support applications to measured vector mgm

- to compare with observations
- to invesigate the field topology associated with CME events
- to study flux emergence, energy and helicity build-up
- as initial condition of MHD simulations
- ...

which are, however, not force-free compatible ...

UCL MSSL

4. Observations as boundary conditions

Vector magnetograms

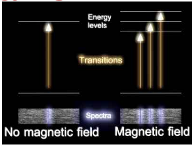

Courtesy of the University of Birmingam, and Google

Physical effect

- Zeeman and Hanle effect $\Longrightarrow$ level splitting emission by ambient magnetic field
- Emission is characterized by Stokes parameters (IUQV: intensity, two linear, circular)
- which are related to the ambient field by (weak field approx.) $B_l \propto V/I$ and $B_t \propto \sqrt{(Q^2 + U^2)}/I$
- The linear polarization are defined modulo a 180° rotation

Measurements

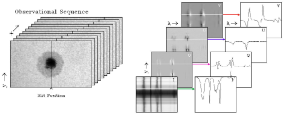

Courtesy of B. Lites

- In *e.g.*, Hinode/SP, the slit scans the FoV
- In each pixel of the slit, Stokes profiles are sampled as a function of λ (higher sampling means higher spectral resolution)
- Sampled Stokes profiles are fit with (semi) analytical emission models (requires a model of the atmosphere, *e.g.*, Milne-Eddington)
- From the best-fitting synthetic Stokes profiles the ambient magnetic field is estimated (inversion)
- The inversion procedure is not well-posed mathematically (Del Toro Iniesta & Ruiz Cobo, Sol.Phys 1996)

Properties of the resulting field

- The orientation of the transverse field is intrinsically undetermined (180° ambiguity)
- The error on B_t is intrinsically about one order of magnitude larger than on B_l
- Specific emission lines of particular elements are chosen according to magnetic sensitivity
- Measurements are on a iso-τ surface, not on a iso-height surface
- Contributions from plasma at different heights may sum up (*e.g.*, in penumbrae)

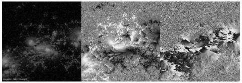

Magnetic field strength, inclination, and azimuth from Hinode/SOT of 14 Feb 2011

UCL MSSL

All above is very qualitative: See, *e.g.*, Landi degl'Innocenti 1994 and Lites JGR 2000 for details

Influence of inversion models

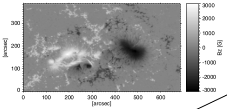

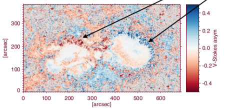

Large asymmetries in the V-Stokes profiles are the signature of steep gradients in the physical parameters (Sankarasubramanian and Rimmele 2002)

The inversion code must be set up to take into account them (a large number of nodes in z)

This is just an example highlighting the importance of customizing the inversion code and its set up

Different inversion model may severely impact on the magnetic field values and, hence, on extrapolations

The fine tuning of the parameters of the code is usually a very long and difficult task

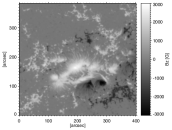

Hinode standard **MERLIN** inversion downloaded from database

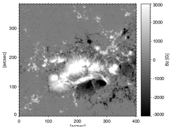

Custom inversion using the **NICOLE** code (Socas Navarro 2014). The vertical gradients are taken into account.

T, v, Bz, Bx, and By are all inverted on a multi-node grid.

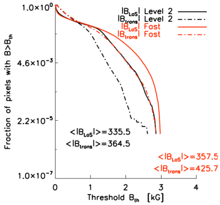

UCL MSSL

Removal of the 180° ambiguity

The transverse components $\vec{B}_t^{\rm obs}$ is measured in amplitude and direction but not in orientation

$\Longrightarrow$ 2D problem where only the sign of $B_t^{\rm obs}$ is to be determined. Several methods, based on

- comparing $B_t^{\rm obs}$ to a reference field or direction
- minimizing the vertical gradient of the magnetic pressure
- minimizing the vertical current density
- minimizing some approximation to $\vec{J}$
- minimizing some approximation to $\vec{\nabla} \cdot \vec{B}$

are discussed and compared in a test using model vector fields in Metcalf *et al.*, Sol.Phys 2006.

Acute angle method Local: The correct orientation of the observed $\vec{B}_t^{\rm obs}$ is the one that forms an acute angle with the local potential field $\vec{B}_t^{\rm pot}$

$$\vec{B}_t^{\rm obs} \cdot \vec{B}_t^{\rm pot} > 0$$

- Fast and simple
- Few variations (*e.g.*, use a LFFF rather than PF)
- Rate of success ranging from 64% to 84% pixels of correct removal
- Often used as first step of more elaborate methods

Minimum energy method Nonlocal: Minimize a pseudo-energy functional

$$E = \sum_{\rm mgm} \left(|\vec{\nabla} \cdot \vec{B}| + |\vec{J}| \right)^2$$

$\min(|\vec{\nabla} \cdot \vec{B}|)$ for consistency and $\min(|\vec{J}|)$ to reduce small scales. Minimize the upper bound of energy

- Global minimum found using simulated annealing
- Use local best-α LFFF to compute $\partial_z B_i$ in E
- Best performing algorithm (up to 100% pixels right)
- Currently used in the standard data production of SDO/HMI and Hinode/SP

Many minima are possible $\Longrightarrow$ not well posed

Inclusion of (simulated photon) noise and spatial resolution (Leka *et al.*, Sol.Phys 2009)

- Pixels with low signal/noise are mostly affected
- Noise and unresolved structures induce errors in the 180° ambiguity resolution, but only local ones
- Suggested order: inversion of spectra $\Longrightarrow$ 180° ambiguity resolution $\Longrightarrow$ binning to lower resolution, if necessary

Errors on the removal often appears as ridges of J_z

UCL MSSL

Heliographic transformation

Unless the (small) FoV is at the center of the solar disk, the LoS is not $\perp$ surface
$\Longrightarrow$ a RS transformation is required

Use (linear) transformation from image to heliographic (Gary & Hagyard Sol.Phys. 1990)

$$\vec{B}^{helio} = \vec{A} \cdot \vec{B}^{\mathrm{image}}$$
$$\vec{x}^{\mathrm{helio}} = \vec{c} \cdot \vec{x}^{\mathrm{image}}$$

$\vec{A}(B_0, B, L - L0, P)$ vector rotation matrix and $\vec{c}(B_0, B_c, L_c - L0, P)$ is a coordinate transformation, expressed in terms of lat/lon (B, L) of each pixel and of the image center (B_c, L_c).

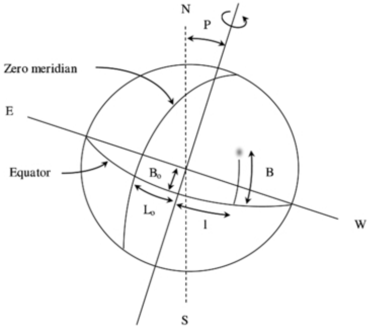

- No sphericity effect (zeroth order in 1/R)
- The RS transformation mixes the observed longitudinal and transverse components (large errors propagates)
- Already 10° off disk center there are visible effect on the location and shape of the PIL (K.D Leka priv. comm.)
- All components are required. If only the LoS is available, a radial field is normally assumed

UCL MSSL

Are mgm a consistent BC?

Example of $\alpha = J_z/B_z$ in AR 11158 (SDO/HMI data)

- $< |\alpha| > \simeq 0.7$ Mm^{-1}
- max($|\alpha|$) $\simeq 10$ Mm^{-1}
- Alternating sign (*e.g.*, penumbrae, see *e.g.*, Gosain *et al.*, 2014)

Threshold for α computation: $|B_z| > 0.05\,\max(|B_z|)$

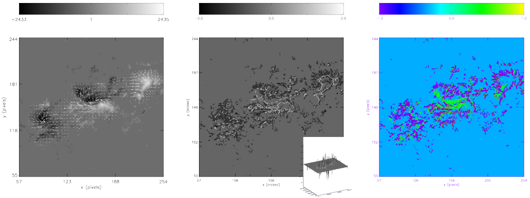

Vector mgm, α, and sign of α

Spiky and noisy, with “fibril”-like structures in penumbrae (artifacts of SP inversion?)

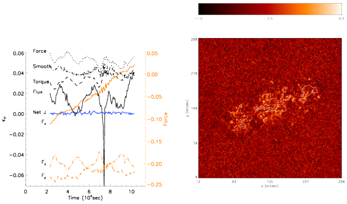

Left: Forces in time (analogous to Sun *et al.*, 2012)

Right: $J_z - J_z^{\mathrm{rotated}}$

Time evolution of forces shows

- 6-hours oscillations (satellite?)
- longitudinal dependence of F_x (Higher order projection effects? Noise?)

Also J_z has large variations (up to 40%) depending on the RS employed to compute it (noise, unresolved structures?)

UCL MSSL

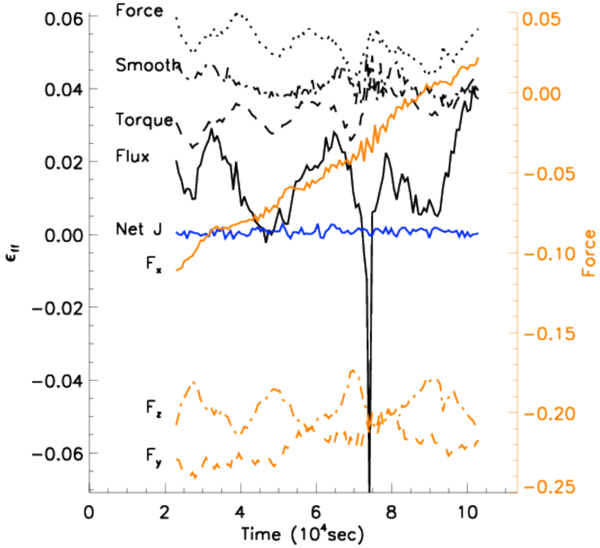

Force
Smooth
Torque
Flux
Net J
F_x
F_z
F_y
0.06
0.04
0.02
0.00
−0.02
−0.04
−0.06
ϵ_{ff}
0.05
0.00
−0.05
−0.10
−0.15
−0.20
−0.25
Force
0
2
4
6
8
10
Time (10^4sec)

UCL MSSL

Extrapolation of nonFF mgm

Combined effects finite-β origin, non-planarity, noise, inconsistency, errors in the 180° ambiguity removal, ...

Looking at Lorentz forces on the mgm, *e.g.*,

$$\mathcal{F}_x = -\frac{\int_{mgm} B_x B_z \, dxdy}{\frac{1}{2}\int_{mgm}(B_x^2 + B_x^2 + B_z^2)\, dxdy}$$

	Force	Torque
nopp	0.127	0.133

Hinode/SP mgm of AR10978 13 Dec 2007

⟹ mgm not FF compatible. What are the consequences on NLFFF extrapolations?

Each method uses the BC differently, so different consequences. However, as a trend

- Non force-free solutions (high values of CWsin)
- Lower energies (with respect to FF BC)
- Bad match with observations
- For methods using $\vec{B}$ rather than $\vec{A}$, pathological solutions with $E < E_{\rm pot}$ may occur (!)

(see *e.g.*, Schrijver *et al.*, ApJ 2008)

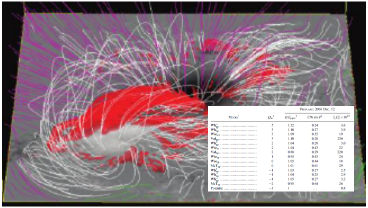

Extrapolation metrics (GR, OP, MF methods) and GR fl of AR10930 (Schrijver *et al.*, ApJ 2008)

UCL MSSL

Negative free energy?

Energy decomposition into solenoidal and nonsolenoidal contributions

- Unphysical: $E < E_{\mathrm{p,s}}$
- $\vec{\nabla} \cdot \vec{B}$ max (combined) error 18% (13%)

	E (10^{33} erg)	($E_{\mathrm{p,s}}$	$E_{\mathrm{j,s}}$	$E_{\mathrm{j,ns}}$	E_{mix})/E
no-pp	1.56	1.03	0.10	0.05	-0.18

MF NLFFF of AR10978 13 Dec 2007. (ns)/(s):non/solenoidal, (p):potential, (j): current

$\Longrightarrow$ The extrapolation of nonFF mgm can lead to non-physical solutions if $\vec{\nabla} \cdot \vec{B}$ too high

Energy of non-solenoidal fields (Valori *et al.*, A&A 2013)

For a given magnetic field $\vec{B}$ in a finite box, solve numerically

1. Split potential from current-carrying in $\vec{B}$

$$\vec{B} = \vec{B}_{\mathrm{J}} + \vec{\nabla}\phi\,, \qquad \text{where} \qquad \begin{cases} \Delta\phi = 0 \\ (\partial\phi/\partial\hat{n})|_{\partial\mathcal{V}} = (\hat{n}\cdot\vec{B})|_{\partial\mathcal{V}} \end{cases}$$

2. Split solenoidal from non-solenoidal in $\vec{B}_{\mathrm{J}}$

$$\vec{B}_{\mathrm{J}} \equiv \vec{B}_{\mathrm{J,s}} + \nabla\psi\,, \qquad \text{where} \qquad \begin{cases} \Delta\psi = \vec{\nabla}\cdot\vec{B}_{\mathrm{J}} \\ (\partial\psi/\partial\hat{n})|_{\partial\mathcal{V}} = 0 \end{cases}$$

all compatible with the condition $\hat{n}\cdot(\vec{B} - \vec{B}_{\mathrm{p}})|_{\partial\mathcal{V}} = 0$ of Thomson's theorem. Substitute the above field decomposition into $E = \frac{1}{2}\int_{\mathcal{V}} B^2 \mathrm{d}\mathcal{V}$

$$\Longrightarrow \quad E = E_{\mathrm{p,s}} + E_{\mathrm{J,s}} + E_{\mathrm{J,ns}} + E_{\mathrm{mix}} \qquad (2)$$

$$E_{\mathrm{p,s}} = \int_{\mathcal{V}} B_{\mathrm{p,s}}^2 \mathrm{d}\mathcal{V}$$

$$E_{\mathrm{J,s}} = \int_{\mathcal{V}} B_{\mathrm{J,s}}^2 \mathrm{d}\mathcal{V}\,, \quad E_{\mathrm{J,ns}} = \int_{\mathcal{V}} |\vec{\nabla}\psi|^2 \mathrm{d}\mathcal{V}$$

$$E_{\mathrm{mix}} = \int_{\mathcal{V}} (\vec{B}_{\mathrm{J,s}}\cdot\vec{\nabla}\psi + \vec{B}_{\mathrm{p,s}}\cdot\vec{B}_{\mathrm{J}})\,\mathrm{d}\mathcal{V}$$

- All terms in Eq. (2) are positively defined, except for E_{mix}
- For a perfectly solenoidal field, it is $E_{\mathrm{p,s}} = E_{\mathrm{p}}$, $E_{\mathrm{J,s}} = E_{\mathrm{J}}$, $E_{\mathrm{p,ns}} = E_{\mathrm{J,ns}} = E_{\mathrm{mix}} = 0$
- The decomposition is accurate to the extent that, in Eq.(2), the two sides are numerically equal, for arbitrary values of divergence.

UCL MSSL

Mgm modifications

Mgm must be "modified" prior to extrapolation in order to

- improve the compatibility with FF assumption
- remove errors / inconsistencies
- reduce noise and smooth small scales (important for some methods)

Two commonly used strategies

1. **Censoring**: remove particular α values according to some criteria like continuity or smoothness, essentially done by hand (preferred by GR users)
2. **Preprocessing**: use global constrains (preferred by MF and OM users)

UCL MSSL

Preprocessing

Minimize a global functional $L(\vec{B}^{\text{obs}})$ by modifying local values of the mgm such that some necessary FF constrains are better satisfied (Wiegelmann *et al.*, Sol.Phys. 2006)

- FF: From the force-free condition, $\vec{\nabla} \cdot (\vec{B}\vec{B} - \vec{I}B^2/2) = 0$, integrated in the volume above the mgm, a positive-definite functional can be derived

$$L_{force} = \left(\int_{mgm} B_x B_z\right)^2 + \left(\int_{mgm} B_y B_z\right)^2 + \left(\int_{mgm} (B_z^2 - B_x^2 - B_y^2)\right)^2$$

  and analogous expressions L_{torque} for the torque (requires flux balance).

- Smoothness: a smoothing functional L_{smooth} can be devised (*e.g.*, using Laplacian or median operators)
- Limiters: Stay as close as possible to observed values by minimizing $L_{\text{dist}} = \sum_{i=x,y,z} \int_{mgm} (B_i - B_i^{\text{obs}})^2$

The different constrains are combined using Lagrangian multipliers $\mu_i \geq 0$ in a global functional to be minimized

$$L = \mu_1 L_{force} + \mu_2 L_{torque} + \mu_3 L_{\text{dist}} + \mu_4 L_{\text{smooth}}$$

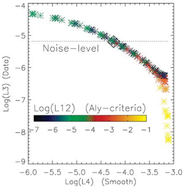

Example of fixing μ_i

- For the minimum of L only the relative weight is important
- $\mu_1 = \mu_2$, no reason to do otherwise
- Fix $\mu_{3,4}$ as the lowest L_{smooth} that keeps L_{dist} below noise level

UCL MSSL

How does PP work?

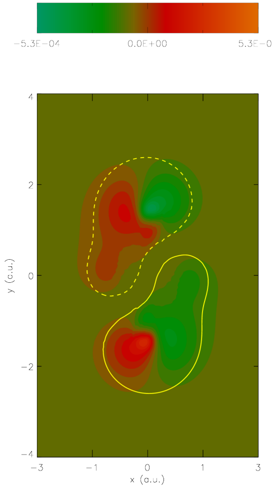

Positive and negative contribution to the integrand of $\mathcal{F}_x$ for the TD

$$L_{force,x} = \mathcal{F}_x^2, \quad \text{where} \quad \mathcal{F}_x = -\int_{mgm} B_x B_z \, dxdy \qquad (3)$$

PP changes B_x and B_z locally in order to decrease $\mathcal{F}_x$. However, for a FF-compatible boundary, it is not the integrand that is small, but its integral

$\Longrightarrow$ PP is inconsistent because it is a local adjustment to fulfil a global constrain

And, analogously to the 180° problem, is not a well-posed problem (the third one!)

Preprocessing

Two implementations (Wiegelmann *et al.*, Sol.Phys. 2006, Fuhrmann *et al.*, A&A 2007) that differ for

- normalizations of L_i, which reflect on different employed μ_i values
- different forms of $L_{\rm smooth}$
- Different strategies of minimization of L:
  - (fast) iterative Newton method $B_i \longrightarrow B_i - \mu dL/dB_i$ in each node
  - (slow) simulated annealing method for global minimum and inclusion of errors' map

See Fuhrmann *et al.*, A&A 2011 for a comparison of the two implementations.

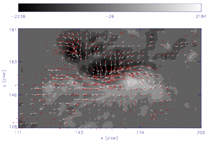

Difference between PP (red) and nonPP (white) transverse component in the core of AR11158

However, preprocessing

- enforces global constraints by means of local modifications
- does not know anything about field lines' connectivity
- limited to the first two moments of the Lorentz force (necessary conditions only)
- μ_i fix the relative importance of each L_i, and need be determined case by case, or at least instrument by instrument (Wiegelmann *et al.*, Sol.Phys. 2012).

$\Longrightarrow$ It can produce FF-compatible BC that do not correspond to any 3D connectivity

Extrapolation of pp mgm

	Force	Torque
no pp	0.127	0.133
pp	0.0004	-0.002

Hinode/SP mgm of AR10978 13 Dec 2007

Compatibility of BC with FF

PP drastically reduces force and torque
$\Longrightarrow$ mgm is FF-compatible

	E (10^{33} erg)	($E_{\rm p,s}$	$E_{\rm j,s}$	$E_{\rm j,ns}$	$E_{\rm mix}$)/E
no pp	1.56	1.03	0.10	0.05	-0.18
pp	1.63	0.85	0.13	0.07	-0.05

MF NLFFF of AR10978 13 Dec 2007. (ns)/(s):non/solenoidal, (p):potential, (j): current

Energy decomposition into solenoidal and nonsolenoidal contributions

- Reduced $\vec{\nabla} \cdot \vec{B}$ error: max (combined) 7% (2%)
- Physical solution: $E > E_{\rm p,s}$
- However, errors are small but comparable with free energy

$\Longrightarrow$ PP is effective in improving the BC compatibility

For all methods, the extrapolation of PP mgm yields

- More FF solutions (lower values of CWsin)
- Improved match with observations
- Higher free energies (with respect to non-PP)
- No pathological solutions with $E < E_{\rm pot}$

(see *e.g.*, Schrijver *et al.*, ApJ 2008)

$\Longrightarrow$ PP is usually beneficial for NLFFF extrapolations

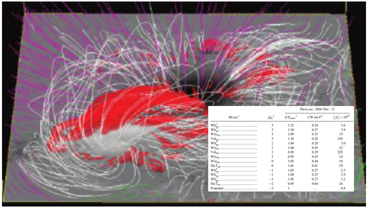

Extrapolation metrics (GR, OP, MF methods) and GR fl of AR10930 (Schrijver *et al.*, ApJ 2008)

Are small scales a problem?

One major difference between test and observed mgm is the presence of important flux on small scales.

- PP *increases* small scales, while, at the same time,
- improving extrapolation

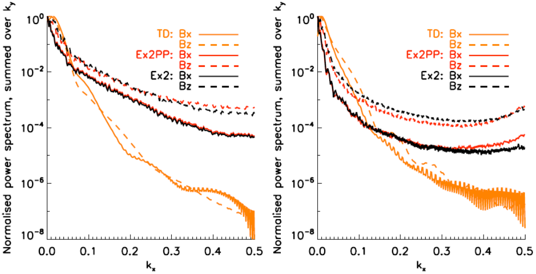

Power spectra of the two-dimensional fields Bx (continuous line) and Bz (dashed line), for the TD (orange), an PP mgm (red),and a non-PP mgm (black)

Small scales are not the obstacle in extrapolation of observed mgm

may influence accuracy of reconstructions depending on the employed numerical scheme (see Valori, Démoulin, Pariat, Masson, A&A 2013)

UCL MSSL

NLFFF extrapolation pipeline

Steps from the AR number to the coronal model:

1. Find spectropolarimetric measurements of suitable quality, size, and cadence (not all instruments are the same)
2. Maps of the magnetic field: inversion of iso-τ spectropolarimetric scans to obtain 2D maps of B_{los}, B_t, and ψ (NWP)
3. Removal of 180° ambiguity (NWP)
4. Heliographic projection and data rebinning on a Cartesian grid
5. Pre-processing, to improve the mgm compatibility with force-free assumption (NWP)
6. Potential field (initial condition for NLFFF extrapolation)
7. NLFFF extrapolation, finally (NWP)

NWP: A mathematically not well-posed problem

Each of these steps involves **models, codes, parameters, and choices**, all of which may severely impact on the extrapolated field

$\Longrightarrow$ Not a press-the-button tool: comparison with observations is mandatory

UCL MSSL

5. Examples of reconstruction in AR

Emergence and evolution of AR11024

Appearing as a tiny bipole on the east limb on 29 June 2009, at about -27° latitude

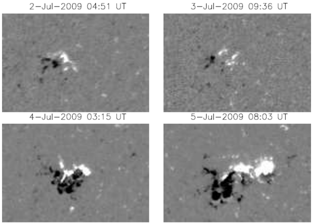

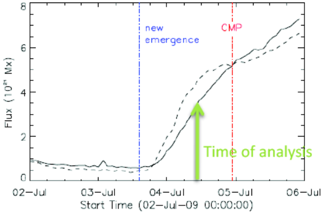

MDI LOS, saturated at 300G (movie at 500G), and time evolution of the emerging positive (—) and negative (- -) magnetic flux

- Positive leading, negative following (dispersed) polarity, mid-scale mixed polarity area in between
- Relatively quiet emergence until suddenly main phase started on 4 July
- Large tilt of new emerging bipoles
- Dominanlty westward flow on positive polarity, southward on negative

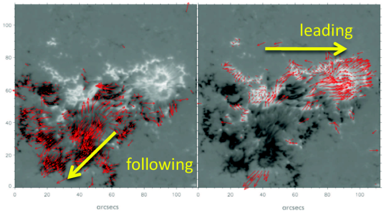

Photospheric flow horizontal velocities (up to 3 km s⁻1) on negative (left) and positive (right) polarities derived from LCT analysis of NFI on 4 July from 12:00 to 13:00 UT

UCL MSSL

Emergence and evolution of AR11024

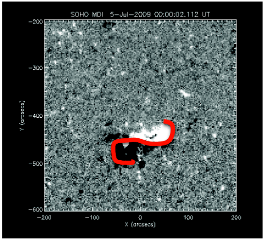

MDI LOS on 05 July 2009, saturated at 300G

- Polarity elongation along the neutral line during the main phase of emergence (starting on 4 July) $\Longrightarrow$ "magnetic tongues" or "magnetic tails"
- from 7 July onward, again bipolar configuration (tongues are retracted)

Interpretation of tongues as

- emergence of azimuthal field (magnetically connected)
- indicate sign of helicity (in this case $H < 0$)

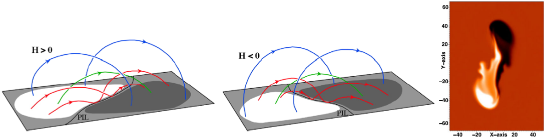

Tongues in a cartoon (Luoni et al. 2011) and in 3D MHD simulations (Archontis and Hood 2010)

Sea-serpent emergence

At the time of main emergence the AR was observed by *Hinode*.

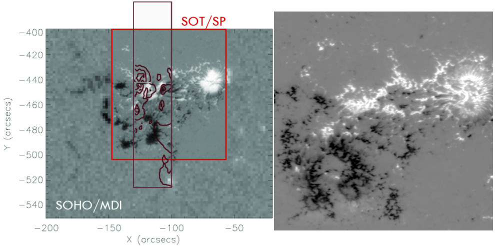

LOS SOT/SP overlaied onto MDI, and NFI LOS between 12 and 13UT

- within the Hinode FoV, 15% excess of positive flux
- Small scale cancellation/cohalescence of opposite/like polarities

Interpreted as the emergence of serpentine field lines (Schmieder et al., 2000): specific relation between the motion close to the PIL, and Ω/U type of field lines.

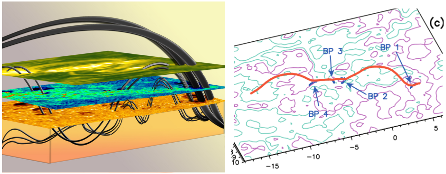

Cartoon (Vargas Domínguez et al. 2011) and linear extrapolation (Pariat et al. 2004) of serpentine emergence

UCL MSSL

Coronal magnetic structure

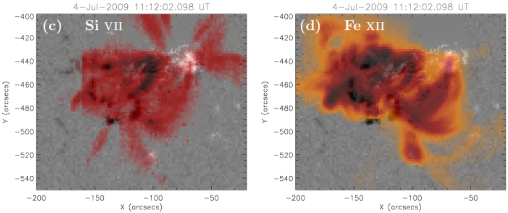

EIS Si VII and Fe XII on 4 July at 11:52 UT,

in reverse colours, overlaied onto MDI

- Sunspot connection
- Internal brightening of tongues connection

- XRT: reconnection fl in between sunspot connection and tongues connection
- Interpreted as rearrangement of emerging magnetic field by reconnection, from small to large scale (e.g., Harra et al 2011),
- eventually leading to the final bipolar structure after 7 July.

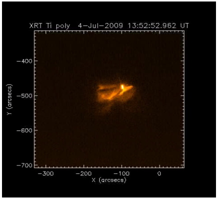

XRT at 13:52 UT (movie: 11:50 - 12:30 UT)

Extrapolation properties

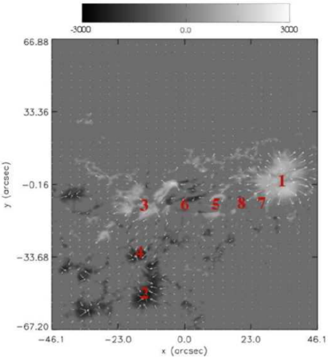

Input: SOT/SP level 2 vector magnetogram
4 July 11:58 until 12:34 UT

- with 180° ambiguity resolved with ME (Leka et al., 2009)
- in heliographic plane, to remove projection effects (AR latitude $\simeq -27°$)
- preprocessed, to reduce forces and torques, with max changes of ± 150 G on $B_{x,y}$ and ± 50 G on B_z
- 293x424 nodes with 0.32" uniform resolution

Output: 3D, force-free model of the coronal magnetic field above it ($\sim$ 100"), with

- $\sigma_J \equiv \int dV\, |\vec{J}_\perp| / \int dV\, |\vec{J}| = 0.11 \Longrightarrow$ (relatively) good force-free
- $< |f_i| >= 3 \times 10^{-4}$, where $f_i \equiv (\int_v dv \vec{\nabla} \cdot \vec{B})/(\int_{\partial v} dv |\vec{B}|) \Longrightarrow$ good divergence-free

$\Longrightarrow$ consistent force-free extrapolation[4]

[4] Valori *et al.*, Sol. Phys. **278** vol.1 (2012)

UCL
MSSL

Large scale connectivity

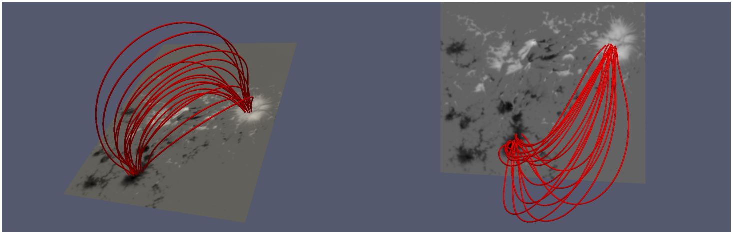

Selected field lines starting in the umbra, in 3D view and in projection on the plane of the sky

Fls connect the sunspot almost exclusively with the southern negative polarity, matching in projection EIS Fe XII.

⟹ original connection of the firstly emerged sunspot pair.

Tilt of the AR possibly due to the emergence of a non-planar flux rope

Right: EIS Fe XII in reverse colours overlaid on MDI

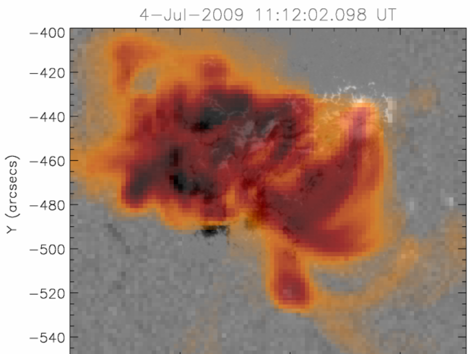

UCL MSSL

Connectivity between tongues

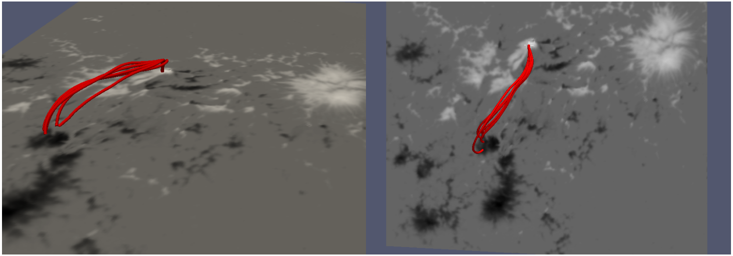

Selected field lines starting in the core of the positive tongue, in 3D view and in projection on the plane of the sky

Sheared field lines connect the elongations of the polarities along the PIL, matching in projection EIS Si VII.

⟹ what were identified as tongues (or tails) from photospheric signatures are indeed magnetically connected

Right: EIS Si VII in reverse colours, overlaid on MDI

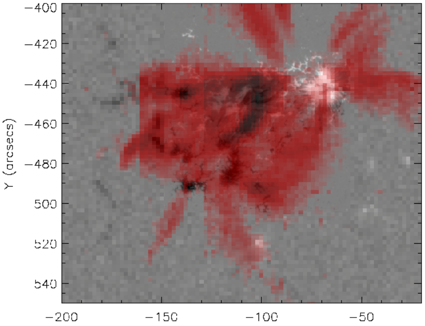

Serpentine field lines

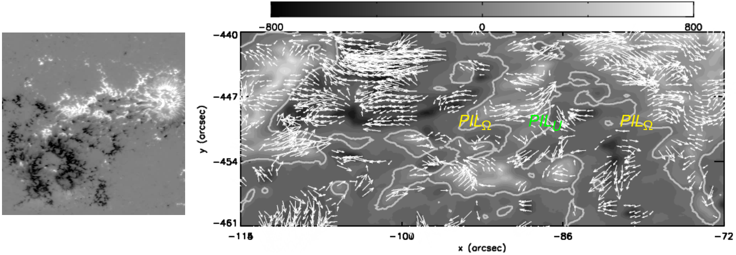

NFI LOS between 12 and 13UT, and LCT flow map in the emerging area

- Ω-loops (resp., U-loops) above PIL characterized by diverging (resp., converging) flows
- Bald patch reconnection creating dipped field lines encompassing adjacent polarities (Pariat et al., 2004)

⟹ Sea-serpent emergence, indeed

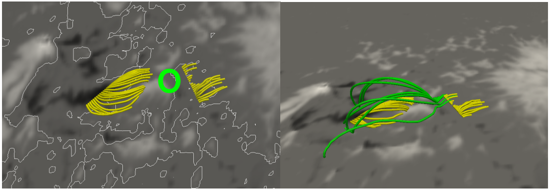

Emerging sea-serpent associated with diverging motion (yellow), and BP-reconnected field lines associated with converging motions (green), starting above the green circle

UCL MSSL

From emergence to AR-wide

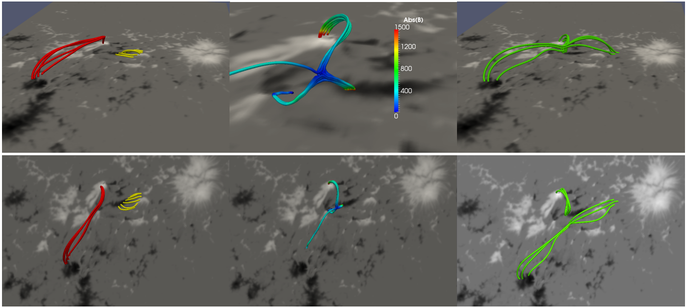

Tongue (red) and sea-serpent (yellow) field lines before reconnection, null point, and reconnected (green) field lines

- Emerging serpentine field lines (yellow) reconnect at the null point with the tongue structure (red)
- forming the green (reconnected) field lines matching XRT observations
- Null point (belonging to a QSL) position in between matches peak location of RHESSI emission between 12 and 12:30 UT

⟹ Example of reconfiguration of emerging flux to AR-scales by successive reconnections

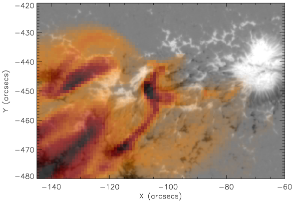

XRT (Ti poly) at 11:52UT in reverse colours overlaid on MDI

UCL MSSL

From emergence to AR-wide

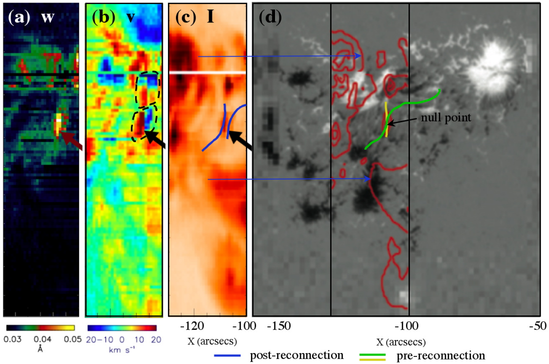

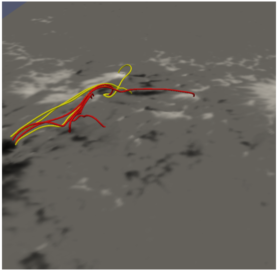

Combined panels on the left: EIS raster of spectral line width (a), Doppler velocities (b), intensity (c) of EIS Fe XII, SOT magnetogram with EIS intensity isocontoures overlaid. Dashes on panel (b) indicates the two dual featuresassociated with nulls. Right: selected field lines showing the two connected null points.

- Uncommon, strong blue/red shifted dual features in the AR core
- can be associated with reconnection outflows
- position of the dual features is matched by two connected null points

⟹ NLFFF extrapolation yields detailed reconstructions which allow the interpretation of complex observations

UCL MSSL

Global metrics

Energy: $E_m = 2.1 \times 10^{33}$ erg =

- 2.8×10^{32} erg of free energy (13% excess of potential field energy)

$\Longrightarrow$ This would be enough to power even X-class flares, but only B and C class flares were detected in the following 3 days.

Relative magnetic helicity: $H_M = -1.1 \times 10^{42}$ Mx^2 =

- -0.05 in units normalized with the magnetic flux

$\Longrightarrow$ Opposite in sign to the statistical hemispheric rule, but in agreement with the observed magnetic tongues.

The gauge-invariant, relative magnetic helicity and the free energy are computed with respect to the potential field having the same distribution of normal field at all six boundaries of the considered finite volume (extension to finite volumes of DeVore ApJ **539** (2000)).

UCL MSSL

Case study conclusions

Employing NLFFF extrapolation during the main phase of emergence of AR11024 we obtained a validation, at all relevant scales simultaneously, of the current understanding of the flux emergence process, as inferred from its manifestations at photospheric and low-coronal heights.

In particular, we found

- Connections of the sunspot pair and between magnetic tongues, and relate them to EIS multi-temperature observations.
- Evidences of the sea-serpent emergence, and relate it to the emergence and flux cancellation processes that are observed in the motion of small magnetic polarities.
- Locations where reconnection occurs in the corona, transforming short serpentine field lines into long-range connectivity across the whole AR, and relate them to reconnection signatures as captured by XRT, RHESSI, and by EIS scans showing localized dual blue/red shifted velocity.
- Helicity and energy estimations coherent with observed evolution.

(Valori *et al.*, Sol. Phys. **278** vol.1 (2012))

Conclusion: NLFFF modeling, in spite of its limitations, is able to provide a realistic description of the coronal magnetic field.

UCL MSSL

Circular ribbon

Circular ribbon flare event

AR 11324 on October 22, 2011

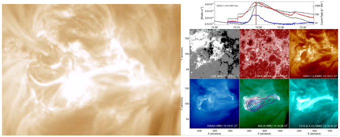

Circular ribbon flare in several SDO/AIA lines

Typical signatures of null-point reconnection

- -ve parasitic within +ve polarity
- Co-temporal inner/outer brightening at the spine's anchoring locations with 1D elongation
- Semi-circular ribbons patches, counter-clock brightening R1-R2-R3

Null-point cartoon of the assumed underline topology

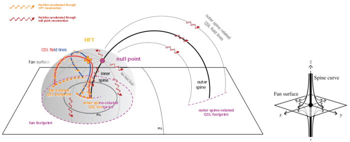

Coronal null-point cartoon (Reid 2012) and a Null Point (Priest 2002)

Not entirely fitting the cartoon model

- Confined event
- Pre-flare brightening of inner structures
- Multi-peaked AIA light curves (not related to eruption as in Sun 2013)
- Post-flare loops above the null rather than under the fan

Next step: Magnetic field modeling based on observations

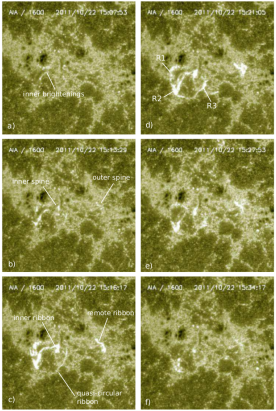

AIA 1600 Å

UCL MSSL

MF structure: Global view

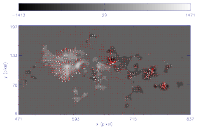

Preprocessed transverse field

⇒ Input: 1", disambiguated, preprocessed SDO/HMI v-mgm
(PP of $\vec{B}_{\rm tr}$ limited to max(50%;100 G))

3D coronal MF : Output ⇐
(40% perpendicular current and 9% non-solenoidal field, typical of HMI)

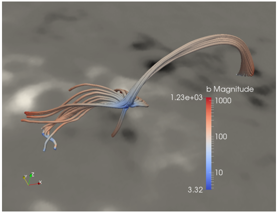

NLFFF fan/spines qualitative structure

Advanced tools for investigating flare/topology relation

Use Quasi-Separatrix Layers to identify the MF's topological elements
QSL: volumes of high values of the connectivity gradients (squashing factor Q), see *e.g.*, Demoulin 2006

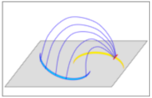

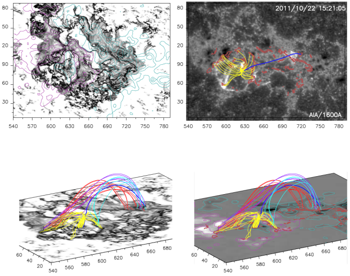

QSL topology study

- Spines/fan global structure
- Unprecedented agreement between observed brightening of
  - QSL on circular ribbon at fan base
  - inner and remote kernels with QSLs at spines' footpoints (!)
  - QSL halo around outer spine and fan

Great matching, but what about flare evolution?

Flare evolution(*)

Use NLFFF extrapolation to associate topological elements to AIA plasma emission

First stage: Activation

QSL analysis reveals the presence below the fan under the null point of

- Complex QSL system with (5!) anchoring on AIA-1600 Å brightening (IS to R1/R2)
- similar in structure to the AIA strands
- Surmounted by a flux rope (R1 to IS)

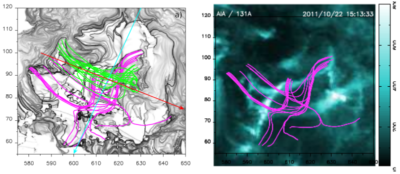

Inner QSLs and flux ropes, and AIA

Interpretation: Inner-QSL internal reconnection as possible flare driver

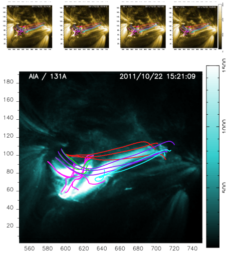

Second stage: Null-point reconnection

This event was **non-eruptive** $\Longrightarrow$ topology largely preserved

- northward, ⊥-PIL ribbon motion, co-temporal with
- AIA-131 Å (short) flux rope and (long) QSL/outer spine FLs

$\Longrightarrow$ Flux from inner to outer domains adding flux *above* the null

Interpretation: Post-flare loops due to reconnection between flux rope and outer QSL field lines at the null (Pariat 2009) followed by slip-running regime at the outer/inner spine QSL halos

(*) CHEAT ALARM: FF equilibrium $\Longrightarrow$ just one snapshot, no evolution!

UCL MSSL

Flare evolution$^{(*)}$

EUV late phase: AIA light curves shows 3 groups of peaks at 16, 26 and 71 minutes after main flare, with delays from hot to cold lines

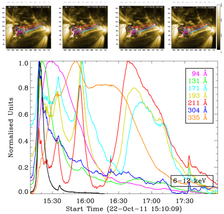

SR reconnection at the null and AIA light curves

- Loops at 335/171/211 Å are co-spatial $\Longrightarrow$ same origin (differently from Woods 2011)
- associate each group to a structure in the magnetic field
  - flux rope
  - R3 to outer spine
  - R2 to outer spine
- within each group, cooler lines peak later
- among groups, shorter connections cool faster

Interpretation: Late EUV evolution due to cooling of post-flare loops created during the main flare episode

Interpretation of the entire evolution of a complex, not fully conventional circular flare ribbon event

$^{(*)}$ CHEAT ALARM: FF equilibrium $\Longrightarrow$ just one snapshot, no evolution!

UCL MSSL

Summarizing

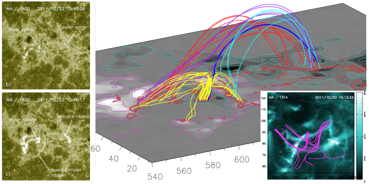

Brightening sequence in AIA 171, NLFFF, and FR

NLFFF matches observations with **great accuracy**

- Non-standard inner bright structure at the position of complex QSL under fan (activation)
- Inner/outer brightening at the spine's anchoring locations, and at the embedding 1D-QSL
- Semi-circular ribbons patches at QSL positions

NLFFF helps **gaining insight into complex observations**

- This event was **non-eruptive**
  $\Longrightarrow$ standard circular ribbon models are inadequate
- Usual null point reconnection is likely
  $\Longrightarrow$ but reconnection adds flux *above* the null
- Cooling events of separate structures from main flare
  $\Longrightarrow$ can explain multiple peaks in light curves
- Provides access to estimations of **free energy and helicity**

(Masson, Pariat, Valori *et al.*, ApJ in preparation)

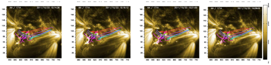

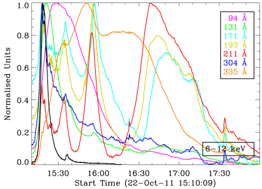

Slip-running reconnection at the null (top) and AIA light curves (bottom)

However, NLFFF is still not entirely quantitative because inaccuracies of observations and methods are still unaccounted for

UCL MSSL

Helicity in a box: a new method

Aim: Gauge-invariant, relative magnetic helicity for application to **finite** domains

Method: use the freedom you have got

For the extrapolated $\vec{B} = \vec{\nabla} \times \vec{A}$ and the potential $\vec{B}_p = \vec{\nabla} \times \vec{A}_p$ fields, the relative helicity (Berger and Field (1984), Finn and Antonsen (1985))

$$H = \int_{\mathcal{V}} d\mathcal{V} \, (\vec{A} + \vec{A}_p) \cdot (\vec{B} - \vec{B}_p) \tag{4}$$

is gauge invariant if $(\hat{n} \cdot \vec{B})|_{\partial\mathcal{V}} = (\hat{n} \cdot \vec{B}_p)|_{\partial\mathcal{V}}$
$\Longrightarrow$ compute $\vec{B}_p = \vec{\nabla}\phi$ by solving numerically $\Delta\phi = 0$ with the above Neumann conditions on all six boundaries of $\mathcal{V} = (x_1, x_2) \times (y_1, y_2) \times (z_1, z_2)$. In order to compute $\vec{A}$ and $\vec{A}_p$ follow DeVore, ApJ **539** (2000), and choose

$$\hat{z} \cdot \vec{A}_p = \hat{z} \cdot \vec{A} = 0. \tag{5}$$

Integrating directly $\vec{B}_p$ between z and z_2 and $\vec{B}$ between z_1 and z, obtain

$$\vec{A}_p = \vec{a} + \hat{z} \times \int_z^{z_2} dz' \, \vec{B}_p, \qquad \vec{A} = \vec{A}_p(x, y, z = z_1) - \hat{z} \times \int_{z1}^{z} dz' \, \vec{B}, \tag{6}$$

where $a_x = -\frac{1}{2} \int_{y_1}^{y} dy' \, B_{p,z}(x, y', z = z_2)$ and $a_y = \frac{1}{2} \int_{x_1}^{x} dx' \, B_{p,z}(x', y, z = z_2)$.
The limit $z_2 \to \infty$ (and no flux outside the magnetogram) reproduces the formulae in DeVore 2000, including $H = \int_{\mathcal{V}} d\mathcal{V} \, \vec{A} \cdot \vec{B}$.

(Valori *et al.*, Sol. Phys. **278** vol.2 (2012))

UCL MSSL

NLFFF Consortium

NLFFF Consortium

Series of comparative works using models and observed cases (2004-2015)

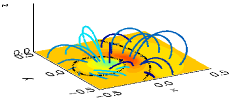

Schrijver *et al.*, Sol.Phys. 2006 Low and Lou test case

- Semi-analytical test case, not quite solar-like (Low & Lou ApJ 1990)
- Successful reconstructions, OM fastest and best performing
- Updates: Amari *et al.*, A&A 2006, Valori *et al.*, 2007, Jiang & Feng ApJ 2012

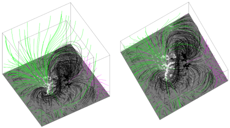

Metcalf *et al.*, Sol.Phys 2008 Numerical test case from flux rope insertion method

- Flux-rope structure in realistic environment (vanBallegooijen ApJ 2004)
- The FR is recovered from pp mgm, but numerical details of implementations impact on reconstruction quality (OM best performing)
- With non-pp mgm the methods basically fail (but also extreme fine scales in α)

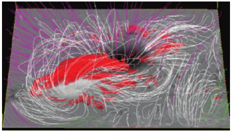

Schrijver *et al.*, ApJ 2008 Application to the Hinode/SOT observations of AR10930

- Pre- and post-flare configurations
- Wide variety of solutions, depending on how each method processes the non-ff boundary
- Relatively poor match with EUV loops, even for the best performing method (GR)
- Update: Canou & Amari ApJ 2010

NLFFF Consortium

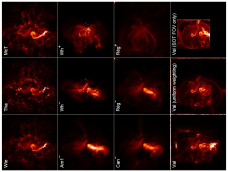

DeRosa *et al.*, ApJ 2009 Application to the Hinode/SOT observations of AR10953

- Embedding in larger LoS mgm
- Poor matching with STEREO-reconstructed loops (possibly not the best test)
- Unsatisfactory dependence of the solution on methods, boundaries, pp, embedding
- PP is necessary but not constrained enough, error maps should be incorporated

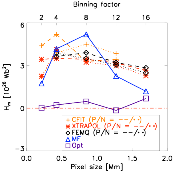

← Higher resolution

DeRosa *et al.*, ApJ 2015 Resolution dependence test on Hinode/SOT observations of AR10798

- Spectra are re-binned at 2, 4, 8, 12, 16 times, then inverted
- Higher free energies with increasing resolution
- Significant spread of helicity values
- All methods change observations of comparable amounts

6. Conclusions

Outlook: Recent developments

Preprocessing codes

- Hα fibrils are believed to be tracers of the (projected) field orientation
  Wiegelmann *et al.*, 2008 extends the PP functional *L* by adding

$$\mu_5 L_{\mathrm{H}\alpha} = \int_{\mathrm{mgm}} \hat{\vec{z}} \cdot (\vec{B} \times \vec{H})$$

  where $\vec{H}$ is a unitary direction of the Hα fibrils (where present), and that is minimized if $\vec{B}_{\mathrm{horiz}} \parallel \vec{H}$
- Maps of measurement errors can be directly used in PP codes that employ simulated annealing as minimization method. First applications are underway

Extrapolation codes

- Maps of measurement errors can be used as confidence maps
  - in iterative GR extrapolations that aim to average the positive and negative solutions (Amari *et al.*, A&A 2010, Whetland *et al.*, ApJ 2011)
  - in a $\vec{W}$ error matrix as an additional term in the OM functional L

$$\int_{\mathrm{mgm}} (\vec{B} - \vec{B}^{\mathrm{obs}}) \cdot \vec{W} \cdot (\vec{B} - \vec{B}^{\mathrm{obs}}) dxdy$$

    which is then minimized during the extrapolation run (Wiegelmann *et al.*, Sol.Phys. 2012)
- Spherical codes (OM: Wiegelmann *et al.*, A&A 2007 GR: Amari *et al.*, A&A 2013, Gilchrist & Wheatland Sol.Phys. 2014, MF: Y. Guo *et al.*, ApJ submitted
- Finite-β codes (OM: Wiegelmann & Neukirk A&A 2006 GR: Wheatland *et al.*, Sol.Phys. 2012)

UCL MSSL

Conclusions

NLFFF extrapolation methods have been substantially improved in the last decade. They

- basically works, sometimes egregiously depending on the method, with FF compatible BC
- are approaching the full resolution of modern measurements, although maybe not yet on full disk
- have been shown to reproduce observed features in a number of cases (see also next talk)
- have been successfully used as a guide to interpret complex observations

However,

- the detailed way in which each method react on non-FF boundary is largely unexplored, hence the variability of solutions from different methods stays unexplained
- vector magnetograms require a preprocessing in order to be used as BC, which is a blind modification of measurements
- and a properly constrained preprocessing remains somehow elusive, due to several different effects and source of errors
- Error maps are still not routinely available and very simple (limited to χ^2 of best fitting profiles plus a confidence measure of the 180° ambiguity removal)

The inclusion of error maps in the extrapolation process might be one possibility of alleviating the problem, but a far more extensive exploitation inversion techniques is necessary:

“A single spectral line contains a richer information than is usually expected”
(Del Toro Iniesta & Ruiz Cobo, Sol.Phys 1996)

UCL
MSSL

NLFFF extrapolation pipeline

Steps from the AR number to the coronal model:

1. Find spectropolarimetric measurements of suitable quality, size, and cadence (not all instruments are the same)
2. Maps of the magnetic field: inversion of iso-τ spectropolarimetric scans to obtain 2D maps of B_{los}, B_t, and ψ (NWP)
3. Removal of 180° ambiguity (NWP)
4. Heliographic projection and data rebinning on a Cartesian grid
5. Pre-processing, to improve the mgm compatibility with force-free assumption (NWP)
6. Potential field (initial condition for NLFFF extrapolation)
7. NLFFF extrapolation, finally (NWP)

NWP: A mathematically not well-posed problem

Each of these steps involves **models, codes, parameters, and choices**, all of which may severely impact on the extrapolated field

$\Longrightarrow$ Not a press-the-button tool: comparison with observations is mandatory

UCL MSSL